

# Analytics and Numerics of Spontaneous Emission of Light at the Optical Event Horizon

Maxime J Jacquet\* and Friedrich König†

*School of Physics and Astronomy, University of St Andrews, SUPA, United-Kingdom*

(Dated: September 14, 2017)

Interest in the study of the scattering of light at a moving refractive index front (RIF) in a dispersive dielectric has recently surged due to the hope of understanding the conditions under which Hawking Radiation may be observed in such systems. Indeed, the kinematics of waves at the RIF are analogous to that on curved space-time geometries. At the horizon, waves of positive and negative norm scatter into each other, which results in the mixing of the creation and annihilation operators of the field and thus in spontaneous emission from the vacuum. In optics, pairwise emission at the horizon occurs in correlated photons of positive and negative frequency. We here present an analytical method that relies on the study of plane wave solutions to a dispersion relation that realistically reproduces the material properties of fused silica or optical fibres, for example, in a time-varying curved one-dimensional background. The method directly and efficiently yields a spectrum, unlike traditional numerical techniques, and can be generalised to considerations of rapidly, smoothly varying background, unlike other analytical methods. We demonstrate that our method enables for readily computing the two essential observables of spontaneous emission at a moving RIF: phase-space and real-space spectra. We compute spectra of light spontaneously emitted at the RIF in the frame co-moving with the RIF as well as in the laboratory frame. We calculate and compute the cross-correlations between mode-solutions in the moving frame and across the spectrum of emission in the laboratory frame. The analytical calculation herein can be used *as is* to predict observables for an optical experiment. The numerical results of this study are the first complete set of phase- and real-space observables calculated for realistic experimental conditions.

## I. INTRODUCTION

Interest in the study of the scattering of light at a moving refractive index front (RIF) in a dispersive dielectric has recently surged due to the hope of understanding the conditions under which Hawking Radiation [1, 2] may be observed in such systems. Indeed, the kinematics of waves at the RIF can be shown to be analogous to that on curved space-time geometries, and in particular at the horizon of black- and white-holes [3]. In both situations, spontaneous emission of particles from the vacuum results from the scattering of waves of positive and negative Klein-Gordon norm into each other at the horizon.

The scattering of positive- and negative-norm waves of the field is rendered possible by time-variations in the curvature of the background on which the waves propagate. In optics, the background of wave propagation is the refractive index. In 2008, a collaboration of the groups of Leonhardt and König at St Andrews demonstrated the feasibility of creating analogue event horizons with a moving refractive index profile in dispersive optical media [4]. An optical event horizon can be created by changing the speed of light (*i.e.*, the refractive index of the medium of propagation) with light itself. For example, a very short and intense laser pulse modifies the index by the optical Kerr effect. Under the pulse, the index is increased. Light will be slowed, and, where the velocity of the waves inside the material is less than the

velocity of the pulse, the front of the pulse acts (for some frequencies) as a black-hole-type horizon that captures light. Phenomenologically, an optical horizon separates two discrete regions: under the pulse where the light is slow and the pulse speed is superluminal, and outside the pulse, where the pulse moves subluminally — in analogy with the motion of space in the vicinity of a black-hole horizon [3, 5]. As in the case of emission at the astrophysical black hole horizon, spontaneous emission from the vacuum in analogue systems results from the mixing of field modes of positive and negative norm at the optical horizons. What is peculiar about the optical setup is that pairwise emission by such a scattering process takes place in correlated photons of positive and negative frequency.

In the inhomogeneous dielectric, the kinematics are dominated by dispersion: this phenomenon regularises the phase singularities at the horizon (dispersion limits the extent to which waves in the medium may shift in frequency) but also renders the wave equations less amenable to analytical techniques. On the other hand, numerical techniques such as finite difference time domain (FDTD) wave packet simulations [6] or Monte Carlo methods [7] can handle the complications due to dispersion and straightforwardly evolve an initial state in time. Such methods are however computationally expensive and do not yield a spectrum directly. There also exist analytical methods, that are restricted to a fixed frequency and situations in which the background varies slowly in comparison with dispersion [8, 9], or some that can only study dispersion relations that are polynomials of low degree [10, 11]. The latter provide numerical

---

\* mj35@st-andrews.ac.uk

† fewk@st-andrews.ac.uk

solutions of the ordinary differential equation (ODE) in position space provided that no exponentially divergent waves exist and that the gradient of background change is low. However, dispersion relations that reproduce the refractive index of materials are usually more complicated than this, and optical experiments typically rely on a large gradient in the background. In particular, when the background change becomes so steep that it can be approximated by a step-like discontinuous function, the solution can be found analytically by matching the plane wave solutions on either side of the interface [12–17].

In this paper, we present an analytical calculation of the Scattering matrix that describes the mixing of waves at a moving RIF. Our method relies on the study of the plane wave solutions to a complicated dispersion relation that realistically reproduces the material properties of fused silica or optical fibres, for example, in a time-varying curved one-dimensional background. As a case study, we consider the specific background geometry of a step-like discontinuity (the RIF) in the refractive index of a dispersive medium. The time-dependence of the background geometry enters via the motion of the RIF in the medium. Studying the step-like geometry is interesting because it allows for de-correlating the effects of dispersion on the one hand, and amplitude of the change in the refractive index on the other hand. Moreover, this geometry has proved able to provide reliable results when the medium parameters do not vary very much between the two homogeneous regions around the step [17] — this certainly is the case in regimes of low-amplitude change in the refractive index [18], as is experimentally realisable [19].

The calculation directly and efficiently yields a spectrum, unlike the above-mentioned numerical techniques, and can be generalised to considerations of rapidly varying background, unlike the above-mentioned analytical methods. Contrarily to the direct solution of an ODE in position space, it is not restricted to a simple polynomial dispersion relation. Throughout the paper, we will use bulk fused silica as an example medium, as in the literature (see, for example, [20] or [18, 21]). Incidentally, this shall allow for checking the present results against the literature [22].

We demonstrate that our analytical method enables the user to readily compute the two essential observables of spontaneous emission at a moving RIF: phase-space and real-space spectra. As an example application, we compute spectra of light spontaneously emitted at the RIF in the frame co-moving with the RIF in the dispersive medium as well as in the laboratory frame (the rest frame of the medium). We also show how to calculate the cross-correlations between mode-solutions in the moving frame, and across the spectrum of emission in the laboratory frame and compute such spectra. The analytical calculation we present here can be used *as is* to predict observables for an optical experiment, and could be generalised to more complicated background geometries. The numerical results of this study are the first complete

set of phase- and real-space observables calculated for realistic experimental conditions.

The paper is structured as follows: in a first section we lay out the field theory of light in a dispersive medium. We describe the interaction of light with matter in a homogeneous medium in the spirit of the Hopfield model [23–25], as was used in [20, 26–28] and [18, 21]. We then move on to studying the configurations of waves in an inhomogeneous medium in which a step-like RIF moves at constant speed. We derive the matching conditions for waves at the interface between the homogeneous media and thus construct Global mode-solutions that describe the *in*-coming and *out*-going fields. We finally use quantum field theory to show that light will be spontaneously emitted at the RIF. In a second section, we present the analytical calculation of the Scattering matrix in terms of the *in* and *out* fields. We then exemplify the use of the Scattering matrix by analytically calculating the laboratory-frame spectral density of spontaneous emission. Additionally, we also show how one can obtain the cross-correlations between mode-solutions in the moving frame, and across the spectrum of emission in the laboratory frame and compute such spectra. In the third and final section of the paper, we demonstrate the abilities of our method by numerically calculating the first complete set of phase- and real-space observables calculated for realistic experimental conditions: we compute spectra of spontaneous emission at the RIF, as well as the cross-correlation maps, in both the moving and laboratory frames.

## II. FIELD THEORY OF LIGHT IN AN INHOMOGENEOUS, DISPERSIVE DIELECTRIC

In this section, we briefly review the field theory developed in [20] and expanded in [21], upon which the analytical calculation presented in this paper is based. We detail how the interaction of light and matter in a uniform dispersive medium is modelled, and identify the eigenmodes and study their properties. We then extend this model to consider an inhomogeneous medium composed of two distinct homogeneous regions (of different optical properties) separated by a moving refractive index front. We proceed to constructing eigenmodes of this nonuniform medium and to describing the scattering of these eigenmodes, that is the mode conversion process at the RIF, by the Scattering matrix formalism. Finally, we quantize the field modes and calculate the photon flux density in terms of the Scattering matrix

### A. Light-matter interaction in a dispersive medium

Let us begin with a short description of the field theory model that will later support the theoretical framework of scattering at a refractive index front (RIF).

In order to describe the interactions of light with a

homogeneous and transparent dielectric medium, we employ a microscopic model inspired by the Hopfield model of Condensed Matter Theory [23], as was first suggested in [25]. We restrict ourselves to a one-dimensional geometry and scalar electromagnetic fields and operate at frequencies sufficiently far from the medium resonances to neglect absorption. Matter, in the model, consists of polarisable molecules, harmonic oscillators of eigenfrequency (resonant frequency)  $\Omega_i$  and elastic constant  $\kappa_i^{-1}$ . In the medium, there is one such harmonic oscillator at each point in space, but since the coupled electromagnetic field has a large wavelength compared to the molecular scale of the dielectric, we can consider the dielectric in the continuum limit [29] and describe the electric dipole displacement by the massive scalar field  $P_i$ . The electromagnetic field (a massless scalar field) in the medium is described by the vector potential  $A(x, t)$  via  $\mathbf{E} = -\partial_t \mathbf{A}$  in temporal gauge. In order to reproduce the refractive index of most materials, we shall henceforth consider a medium featuring three resonances. In the rest frame of the medium — the laboratory frame — the interaction of the electromagnetic field with the three polarization fields of the medium is described by the Lagrangian density [20, 21, 23, 24]

$$\mathcal{L}_{LF} = \frac{(\partial_t A)^2}{8\pi c^2} - \frac{(\partial_x A)^2}{8\pi} + \sum_{i=1}^3 \left( \frac{(\partial_t P_i)^2}{2\kappa_i \Omega_i^2} - \frac{P_i^2}{2\kappa_i} + \frac{A}{c} \partial_t P_i \right) \quad (1)$$

where the inertia of the harmonic oscillators  $P_i$  when subjected to an external drive is  $(\kappa_i \Omega_i^2)^{-1}$ . The term linear in  $A$  in Eq.(1) describes the coupling between the fields. The Lagrangian density accounts for the free space and medium contributions to the field through the first two terms and the sum, respectively. Dispersion enters as a time dependence of the addends of the summation.

The step in refractive index (RIF) is propagating in the positive  $x$  direction at speed  $u$ . It is convenient to express the Lagrangian density (1) in a frame co-moving with the RIF by applying a Lorentz boost

$$\begin{pmatrix} x \\ t \end{pmatrix} = \gamma \begin{pmatrix} 1 & u \\ \frac{u}{c^2} & 1 \end{pmatrix} \begin{pmatrix} \zeta \\ \tau \end{pmatrix}. \quad (2)$$

In this moving frame, the system is stationary — the medium properties are independent of time and the Lagrangian density reads

$$\mathcal{L}_{MF} = \frac{(\partial_\tau A)^2}{8\pi c^2} - \frac{(\partial_\zeta A)^2}{8\pi} + \sum_{i=1}^3 \left( \frac{\gamma^2 (\partial_\tau P_i - u \partial_\zeta P_i)^2 \lambda_i^2}{2\kappa_i (2\pi c)^2} - \frac{P_i^2}{2\kappa_i} + \frac{A\gamma}{c} (\partial_\tau P_i - u \partial_\zeta P_i) \right). \quad (3)$$

By the principle of least action, we obtain the Hamiltonian density by varying the Lagrangian density (3) with

respect to the canonical momentum densities of light

$$\Pi_A = \frac{\partial \mathcal{L}_{MF}}{\partial (\partial_\tau A)} = \frac{\partial_\tau A}{4\pi c^2} \quad (4)$$

and polarisation fields

$$\Pi_{P_i} = \frac{\partial \mathcal{L}_{MF}}{\partial (\partial_\tau P_i)} = \frac{\gamma^2 (\partial_\tau P_i - u \partial_\zeta P_i)}{\kappa_i \Omega_i^2} + \frac{A\gamma}{c}. \quad (5)$$

From the Hamiltonian density follow the Hamilton equations, the equations of motion for the fields [30]. We complexify the massive field obtained from the action of (3) by demanding plane wave solutions of the form

$$V = \bar{V}_{\omega'} e^{ik'\zeta - i\omega'\tau}, \quad (6)$$

where  $V$  is the eight-dimensional field operator  $V = (A \ P_1 \ P_2 \ P_3 \ \Pi_A \ \Pi_{P_1} \ \Pi_{P_2} \ \Pi_{P_3})^T$ .  $k'$  and  $\omega'$  are, respectively, the wavenumber and frequency in the moving frame. We go to Fourier space,  $\partial_\tau = -i\omega'$  and  $\partial_\zeta = ik'$ , and arrive at the Hamilton equations

$$\begin{cases} -i\omega' A = 4\pi c^2 \Pi_A, \\ -i\omega' P_i = \frac{\kappa_i}{\gamma^2 \Omega_i^2} \left( \Pi_{P_i} - \frac{A\gamma}{c} \right) + u ik' P_i, \\ -i\omega' \Pi_A = -\frac{k'^2 A}{4\pi} + \sum_{i=1}^3 \left( \frac{\kappa_i}{\gamma^2 \Omega_i^2} \left( \Pi_{P_i} - \frac{A\gamma}{c} \right) \right), \\ -i\omega' \Pi_{P_i} = -\frac{P_i}{\kappa_i} + u ik' \Pi_{P_i}. \end{cases} \quad (7)$$

Eliminating the fields in (7), simple algebra then leads to the generic Sellmeier (laboratory-frame) dispersion relation of bulk transparent dielectrics:

$$c^2 k^2 = \omega^2 \left( 1 + \sum_{i=1}^3 \frac{4\pi \kappa_i}{1 - \frac{\omega^2}{\Omega_i^2}} \right) \quad (8)$$

where the Lorentz transformations from the laboratory frame to the moving frame was used to identify  $\omega' = \gamma(\omega - uk)$  and  $k' = \gamma(k - \frac{u}{c^2}\omega)$  ( $k$  and  $\omega$  are the wavenumber and frequency in the laboratory frame). This dispersion relation is plotted in Fig. 1: there are eight branches, four with positive laboratory frequency, and their four negative laboratory frequency counterparts, symmetric about the  $k$  axis.

By construction, the (complexified) Lagrangian (3) is invariant under any transformation of the global phase of the dynamic fields. According to Noether's theorem, this continuous symmetry implies a conserved current and, in the moving frame, being the system stationary, the current density is a space-time-independent quantity for the plane wave modes (6) [18]. As a result, the norm of these modes is conserved, and so is the Klein-Gordon scalar product defined on the set of our Hamilton equations generalised to complex values (7)

$$\langle V_1, V_2 \rangle = \frac{i}{\hbar} \int d\zeta V_1^\dagger(\zeta, \tau) \eta V_2(\zeta, \tau). \quad (9)$$

The  $\hbar^{-1}$  prefactor was inserted for normalisation purposes and  $\eta$  is the symplectic matrix —  $\eta = \begin{pmatrix} 0 & I_4 \\ -I_4 & 0 \end{pmatrix}$ ,

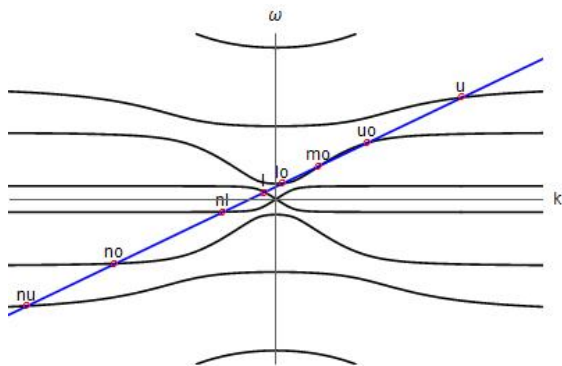


Figure 1. Sellmeier dispersion relation, Eq.(8), with three resonances in the laboratory frame. There are eight branches (black lines). A contour of  $\omega'$  is shown in blue. Their intersection points indicate the modes of propagation in the medium (red circles)

with  $I_4$  the  $4 \times 4$  identity matrix. Note that the scalar product (9) is not positive definite, and thus the norm of all mode solutions — which is inherited from this scalar product — is not necessarily positive. In fact, modes that have a negative frequency in the laboratory frame have a negative norm, whilst modes that have a positive frequency in the laboratory frame have a positive norm, and vice-versa [20]. Thus modes belonging to the upper (lower) half plane of the dispersion relation in energy momentum space (Fig. 1) have positive (negative) norm. As we will see shortly, in the comoving frame, positive-frequency waves with negative norm appear.

### B. Mode configurations at a refractive-index front

In the previous section we presented a canonical model aiming at describing the phenomenology of light and matter interaction in a dielectric medium. We found that mode solutions of the field equations of motion in a homogeneous medium could have positive or negative norm as a function of their frequency in the laboratory frame (the rest frame of the medium). We will now push our study of the system further to describe a non-uniform medium. We consider the simple geometry of a refractive index front (RIF) as shown in Fig.2 in the comoving frame. The medium is composed of two homogeneous regions, separated by the RIF at  $\zeta = 0$ , creating a step in the refractive index. The boundary at  $\zeta = 0$  constitutes an infinitely steep RIF which propagates in a steady and rigid way in the positive  $\zeta$  direction. Phenomenologically, the refractive index of a homogeneous region is described by the dispersion relation (8), with dispersion parameters  $\kappa_{i,R}$  ( $\kappa_{i,L}$ ) and  $\Omega_{i,R}$  ( $\Omega_{i,L}$ ) in the right (left) region. The change in refractive index between the left and right regions is modelled by the step height  $\delta n$ , defined by

$$n(\zeta) = n_L \theta(-\zeta) + n_R \theta(\zeta) = n_R + \delta n \theta(-\zeta) \quad (10)$$

$\theta(\zeta)$  is the Heaviside step function; and illustrated in Fig.2. Thus the index change is described by the scaled Sellmeier coefficients  $\kappa_{iL} = \sigma \kappa_{iR}$ , and  $\Omega_{iL}^2 = \sigma \Omega_{iR}^2$ , where  $\sigma \approx 1 + \frac{2n_R \delta n}{n_R^2 - 1}$  and  $n_R$  is the refractive index on the right side [20, 21].

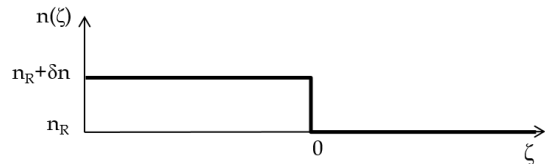


Figure 2. Sketch of the RIF in the moving frame: there are two homogeneous regions of uniform refractive index on the left and right of a dielectric boundary of height  $\delta n$ .

We saw earlier that, in the moving frame, the current density for plane wave modes (6) of the field in a homogeneous region is independent from space and time. This implies that energy is conserved in the moving frame, that is the comoving frame frequency  $\omega'$  is a conserved quantity —  $\gamma(\omega - uk) = \text{const}$  in the laboratory frame. This condition is a straight (blue) contour-line of slope  $u$  and  $\omega$ -intercept  $\omega = \omega'$  in Fig.1. In terms of our field theory, this means that we can identify the modes of propagation of the field subject to the dispersion relation (8) in both regions for a given  $\omega'$ . Thus solutions of fixed  $\omega'$  are found at the intersection points between a line of constant  $\omega'$  with the various polariton branches in the dispersion diagram (red circles in Fig. 1). The dispersion relation (8) is an eighth order polynomial, thus there exists a set of eight  $(\omega, k)$  solutions, modes of oscillation of the field  $V$  that have the same energy in the moving frame. Note that we consider only positive comoving frequencies  $\omega'$  low enough for the blue contour line  $\omega' = \text{const}$  not to intersect with the top dispersion branch. On either side of the RIF, we either find eight propagating modes or six propagating modes and two exponentially growing and decaying modes, respectively, that take on complex  $\omega$  and  $k$ .

We now study the nature and configuration of modes at the RIF for all comoving frequencies  $\omega'$ . After [20] and [18, 21], we know that only the positive-norm optical modes change in nature (complex or oscillatory) as a function of the comoving frequency  $\omega'$ . Thus studying their configurations allows for fully characterising the nature of the system (*i.e.*, knowing when the boundary in the refractive index acts as an analogue horizon) and we focus our attention on the configurations of modes belonging to the “middle”-frequency branch in our model (8) (where  $\Omega_3 < \Omega < \Omega_2$ ) (which corresponds to the optical frequency interval) — the *optical* branch.

In particular, consider the positive- and negative-norm optical branches in the moving frame, depicted in Fig.3. The black (orange) curve is the branch on the right (left) side of the RIF. The number of mode solutions depends on  $\omega'$ . On either side of the RIF, there is at

least one propagating optical mode for all  $\omega'$ . There is also a frequency interval over which a line of constant  $\omega'$  (that would be horizontal in Fig.3) intersects three times with the optical branch — there, three propagating modes exist: between the two horizontal dashed black lines and two horizontal dashed orange lines in Fig.3, respectively. Hereafter, these frequency intervals on either side of the RIF are referred to as the *subluminal intervals* (SLIs)  $[\omega'_{minL}, \omega'_{maxL}]$  and  $[\omega'_{minR}, \omega'_{maxR}]$ . On all other branches, of positive or negative frequency, there always exist only one mode — *i.e.*, one oscillatory solution to the equation of motion.

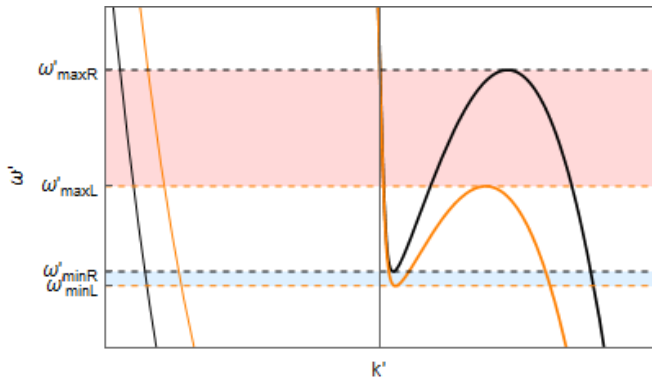


Figure 3. Sellmeier dispersion relation of bulk fused silica in a frame moving at a velocity  $u = 0.66c$ . Part of the optical branch is shown: branches with positive (negative) laboratory frequencies are represented by thick (thin) curves. A curve for zero refractive-index change  $\delta n$  is shown in black, and that for a small change  $\delta n = 0.02$  is in orange. Frequency intervals corresponding to black- and white-hole analogue horizons are shaded in orange ( $[\omega'_{maxL}, \omega'_{maxR}]$ ), and blue ( $[\omega'_{minL}, \omega'_{minR}]$ ), respectively.

Inside a SLI, one of the three mode solutions has a positive comoving group velocity  $\frac{\partial \omega'}{\partial k'}$ . This unique optical mode allows light on the right of the RIF to propagate away from it. This middle optical mode (see Fig.1) on the right is called *moR* in what follows. The other two modes have negative comoving group velocity; they move into the boundary from the right. There is a lower (upper) optical mode denoted *loR* (*uoR*). On either side we can order the modes by the comoving wave number  $k'$  and obtain  $k'_{\omega'}^{loR/L} < k'_{\omega'}^{moR/L} < k'_{\omega'}^{uoR/L}$  (see Fig.3). Beyond the SLI — *i.e.*,  $\omega' \notin [\omega'_{min}, \omega'_{max}]$  — only one propagating mode remains. Two complex-wave-number roots of (8) emerge as pairs of exponentially growing and decaying modes that do not propagate. For  $\omega' < \omega'_{min}$  only mode *uoR/L* remains a propagating mode, whereas for  $\omega' > \omega'_{max}$ , only *loR/L* remains. As stated earlier, and as can also be seen in Fig.3, for all comoving frequencies there is one propagating mode that belongs to the negative optical-frequency branch. This mode has a negative norm and will hereafter be referred to as *noR/L*.

In [21], we used kinematics arguments to show that

the boundary in the refractive index acts as an analogue black-hole horizon for modes of the field over the  $[\omega'_{maxL}, \omega'_{maxR}]$  frequency interval only. Indeed, light may not propagate from the region on the left of the boundary (high refractive index region) to the region on the right (low refractive index region). In kinematic terms, the background on which the waves propagate flows at subluminal speed in the left region, and superluminal speed in the right region: the boundary is the analogue of a black-hole horizon. We found that, for small refractive index change amplitudes ( $\delta n < 0.11$  for bulk fused silica [31]), there exist a further four mode configurations. In particular, over the  $[\omega'_{minL}, \omega'_{minR}]$  frequency interval, the boundary acts as an analogue white-hole horizon. This was latter generalised to all regimes of refractive index change in [18]. The calculation that will be presented in the next section fully accounts for all refractive index change and possible mode configurations. All possible mode configurations are presented on Fig.4: in growing order of comoving frequency, we have —

1.  $\omega' < \omega'_{minL}$ . One optical propagating mode (*uoL/R*), and has negative group velocity in the moving frame, on either side of the boundary.
2.  $\omega'_{minL} < \omega' < \omega'_{minR}$ . On the left of the boundary, there exist three optical propagating modes (*loL*, *moL*, and *uoL*) whilst only mode *uoR* exists on the right. All modes in the inhomogeneous medium have negative comoving group velocity, except for *moL* that has positive comoving group velocity on the left.
3.  $\omega'_{minR} < \omega' < \omega'_{maxL}$ . Three propagating modes (*loL/R*, *moL/R*, and *uoL/R*) exist on either side of the boundary. Mode *moL(R)* has positive comoving group velocity on the left (right) of the RIF, and all other modes have negative comoving group velocity.
4.  $\omega'_{maxL} < \omega' < \omega'_{maxR}$ . Only one mode, with negative comoving group velocity, exists on the left of the boundary, but modes *loL/R*, *moL/R*, and *uoL/R* exist on the right — with negative, positive, and negative comoving group velocity, respectively.
5.  $\omega' > \omega'_{maxR}$ . One propagating mode (*loL/R*) exists on either side of the boundary. All propagating modes exhibit negative group velocities.

In configurations 1 and 5, the increase in the refractive index in the right region does not modify either the nature nor the direction of propagation of the sole optical frequency mode that exists on either side of the RIF: no optical horizon exists. Configuration 2 is more interesting, and its description is novel: light in mode *loL* propagates from the left into the boundary, but cannot enter the right region, because all modes there have negative group velocity. Over the  $[\omega'_{minL}, \omega'_{minR}]$  frequency interval, the boundary acts as a white hole to modes of the

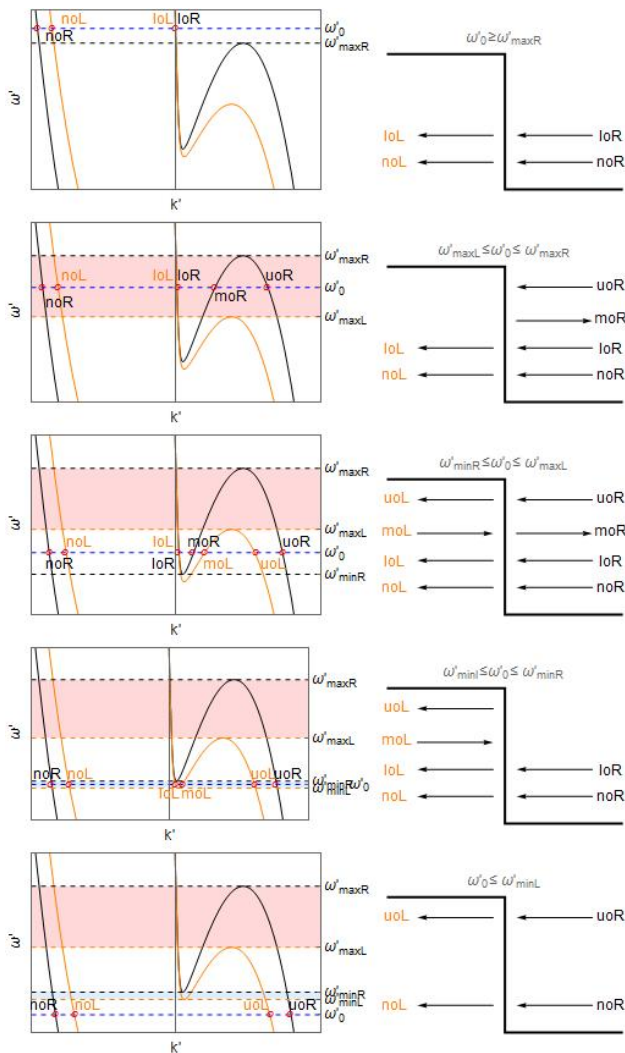


Figure 4. Diagrammatic explanation of the possible mode configurations for positive- and negative-norm optical modes for various comoving frequencies  $\omega'$ , in a regime of low amplitude refractive index change (here  $\delta n = 0.02$ ). Modes are schematically sketched at the step for comoving frequency  $\omega'_0$  (blue dashed line in the dispersion diagrams). The arrows indicate the comoving group velocity of each mode. Modes noL and noR are the only negative-norm optical modes, on the left and right of the step, respectively. All other optical modes have a positive norm. The step acts as a black-hole-like horizon over the orange-shaded interval, and as a white-hole-like horizon over the blue-shaded interval.

field as light can approach but not enter the right region. Symmetrically, over the frequency interval of configuration 4, light experiences a black-hole horizon at the RIF as it cannot propagate to the right from beyond the RIF. Finally, configuration 3 is similar to 1 and 5 in that the step in the refractive index does not affect either the nature or the direction of propagation of the optical modes. It is, however, slightly different from them in that modes with negative and positive group velocity exist on either side of the RIF: although the RIF is not a one-way door

(as in configurations 2 and 4) and thus no horizon exists for waves of this frequency, the situation is somewhat analogous to gravitational disturbances such as gravitational waves. In configuration 2 (4), the region on the right (left) of the boundary corresponds to the inner region, whilst that on the left (right) corresponds to the outer region, respectively, of the analogue horizon. Consider configuration 4: on the left of the boundary, light can only propagate to the left — in only one direction, in analogy with the interior region of a black hole where the space flow is superluminal. In contrast, on the right of the boundary, light can propagate in both directions (in analogy with a subluminal flow of space). The symmetrical analogy holds for configuration 2. This analogy to black- or white-hole physics stems from the disturbance in the refractive index, which plays the same role as the geometrical disturbance in the vicinity of a black hole.

Note that the RIF acts simultaneously as a black-hole, white-hole, and no-horizon boundary (although over different discrete frequency intervals) [18, 21]. In the next section, we will establish the matching conditions for the fields at the interface in the refractive index. This will then allow us to proceed to quantising the field theory: we will quantise for small perturbations (the plane wave modes of the inhomogeneous medium) on a classical geometrical background (the refractive index increase at the RIF). This will reveal how, in total analogy with black hole physics, fluctuations of the quantum vacuum at the RIF give rise to spontaneous emission of light.

### C. Mode matching at the refractive index front

In the previous section, we have derived solutions on either side of the RIF, we now construct "global" solutions, *i.e.*, solutions to the equation of motion that are valid in both regions. These modes correspond to waves scattering at the RIF, and they describe the conversion of an incoming field, even in the quantum vacuum state, to scattered fields in both regions.

#### 1. Mode matching across the boundary

We now proceed to match the asymptotic stationary modes (6) across the refractive index boundary at  $\zeta = 0$ . Since they exist in only one of the two homogeneous regions separated by the RIF, these modes will henceforth be denoted local modes (LMs).

On physical grounds, we consider all fields, conjugate momenta and time derivatives to be finite. By construction of the model, the elastic constant and inertia of the polarisation fields are, respectively, discontinuous and continuous at the interface between the two homogeneous media. In the near-interface region, we gain insight in the behaviour of the fields and conjugate momenta by integrating the equations of motion over time. We begin with the third equation of (7): we integrate with respect to

the spatial coordinate about  $\zeta = 0$  from  $-\epsilon$  to  $+\epsilon$ , taking the limit  $\epsilon \rightarrow 0$ ,

$$\int_{-\epsilon}^{+\epsilon} i\omega' \tilde{\Pi}_A d\zeta = \int_{-\epsilon}^{+\epsilon} \frac{\tilde{A}''}{4\pi} d\zeta + \int_{-\epsilon}^{+\epsilon} \sum_{i=1}^3 \frac{\kappa_i \Omega^2}{\gamma c} \left( \tilde{\Pi}_{P_i} - \gamma \frac{\tilde{A}}{c} \right) d\zeta. \quad (11)$$

All finite terms integrate to zero for the limit  $\epsilon \rightarrow 0$ , thus

$$\int_{-\epsilon}^{+\epsilon} \sum_{i=1}^3 \frac{\kappa_i \Omega^2}{\gamma c} \left( \tilde{\Pi}_{P_i} - \gamma \frac{\tilde{A}}{c} \right) d\zeta \rightarrow 0, \quad (12)$$

and (11) yields

$$\int_{-\epsilon}^{+\epsilon} \frac{\tilde{A}''}{4\pi} d\zeta = 0, \quad (13)$$

$A''$  is finite. Thus the vector potential  $A$  is continuously differentiable:  $A_L = A_R$  and  $A'_L = A'_R$ . Proceeding similarly with the second equation of (7) leads to the condition

$$u \int_{-\epsilon}^{+\epsilon} \tilde{P}'_i d\zeta = 0 \quad (14) \\ \Rightarrow P_{iL} = P_{iR}.$$

That is, the polarisation fields are continuous across the interface. We apply the same process to the fourth equation of (7): all the terms being finite, integrating and subsequently taking the limit  $\epsilon \rightarrow 0$  shows that the  $\Pi_{P_i}$ s are continuous as well. Glancing again at the second equation of (7) and noticing that all the terms except  $P'_i$  are continuous we realise that the spatial derivatives of the polarisation fields are also continuous:  $P'_{iL} = P'_{iR}$ . Finally, turning back to the fourth equation of (7), in which both  $P_i$  and  $\tilde{\Pi}_{P_i}$  ( $k' \Pi_{P_i}$ ) are continuous, we see that the discontinuity in  $\kappa_i$  implies that the term  $\partial_\zeta(u \Pi_{P_i})$  must carry a discontinuity. Equating the Hamilton equations for each side of the step by identifying  $\tilde{\Pi}_{P_iL} = \tilde{\Pi}_{P_iR}$  yields

$$\left( \dot{\tilde{\Pi}}_{P_iL} - u \Pi'_{P_iL} \right) = \frac{-P_{iL}}{\kappa_{iL}}, \\ \left( \dot{\tilde{\Pi}}_{P_iR} - u \Pi'_{P_iR} \right) = \frac{-P_{iR}}{\kappa_{iR}}, \quad (15) \\ \Rightarrow \Pi'_{P_iR} - \Pi'_{P_iL} = \frac{P_i}{u} \left( \frac{1}{\kappa_{iR}} - \frac{1}{\kappa_{iL}} \right).$$

That is,  $\Pi'_{P_i}$  is discontinuous.

To sum up, we have found that the fields and their conjugate momenta are continuous at the boundary. The spatial derivatives of all fields and conjugate momenta are also continuous, with the exception of  $\Pi'_{P_i}$ . Furthermore, looking at the Hamilton equations of motion (7), we see that the finiteness of the temporal derivatives of the fields imply that they are continuous.

## 2. Global Modes of the inhomogeneous medium

We now use the S-matrix formalism to relate incoming and outgoing fields at the RIF. We thus seek bases of *in* and *out* modes that live in the two regions of the inhomogeneous medium and are related by the scattering matrix. These are called global modes (GMs) We construct the GMs  $\mathcal{V}$  as

$$\mathcal{V} = \sum_{\alpha} L^{\alpha} V_L^{\alpha} \theta(-\zeta) + \sum_{\alpha} R^{\alpha} V_R^{\alpha} \theta(\zeta), \quad (16)$$

where  $L^{\alpha}$  ( $R^{\alpha}$ ) describes the strength of mode  $\alpha$  on the left (right) side of the RIF. Half of the coefficients in (16) are constrained by the matching conditions. We consider GMs whose asymptotic decomposition comprises only a single LM with comoving frame group velocity towards (*in*) or away from (*out*) the RIF [10]. Thus there are as many of these GMs as there are propagating local modes. Half of the GMs emerge from a defining LM  $\alpha$  that moves towards the RIF, forming global *in* modes  $\mathcal{V}^{in\alpha}$ . The other GMs are global *out* modes  $\mathcal{V}^{out\alpha}$  if  $\alpha$  is a LM now moving away from the RIF. The LMs are the complete physical (*i.e.*, nondivergent) solutions in the asymptotic regions, thus the sets of  $\mathcal{V}^{in}$  and  $\mathcal{V}^{out}$  modes are two basis sets of modes. Hence the scattering matrix  $S$  is the transformation of modes from the *out* basis to the *in* basis:

$$\mathcal{V}^{in\alpha} = \sum_{\beta} \mathcal{V}^{out\beta} S_{\alpha\beta}. \quad (17)$$

Scattering and spontaneous photon creation occur as the input vacuum state does not correspond to the vacuum state in the *out* basis; that is, the spontaneous emission follows from  $S$ , that governs all mode conversion. In the next section, we will follow the canonical approach introduced in [24], developed in the 1990s in [32–37], and used in [20, 27, 28] and [18, 21] to quantise the global modes and show that, because of the moving disturbance in the refractive index (the RIF), spontaneously particle creation occurs.

## D. Quantum Field Theory

### 1. Creation and annihilation operators of a Global Mode

We postulate the equivalent of the standard equal-time commutation relations on the fields  $A$  and  $P_i$  and thus quantise the local field modes and their momenta:

$$[A(\zeta), \Pi_A(\zeta')] = i\hbar \delta(\zeta - \zeta'), \quad (18)$$

$$[P_i(\zeta), \Pi_{P_j}(\zeta')] = i\hbar \delta_{ij} \delta(\zeta - \zeta'). \quad (19)$$

We expand the field  $V$  on the basis of local frequency eigenmodes

$$V = \int d\omega' \sum_{\alpha} \left( V_{\omega'}^{\alpha} \hat{a}_{\omega'}^{\alpha} + V_{\omega'}^{\alpha*} \hat{a}_{\omega'}^{\alpha\dagger} \right) \quad (20)$$

that are properly normalised with respect to the scalar product (9) under the condition [20]

$$\left| \langle V_{\omega'_1}^{\alpha_1}, V_{\omega'_2}^{\alpha_2} \rangle \right| = \delta(\omega'_2 - \omega'_1) \delta_{\alpha_2 \alpha_1}. \quad (21)$$

Alternatively, we can expand the field over positive frequencies only, including negative-norm modes in the expansion:

$$V = \int_0^\infty d\omega' \left( \sum_{\alpha \in P} V_{\omega'}^\alpha \hat{a}_{\omega'}^\alpha + \sum_{\alpha \in N} V_{\omega'}^\alpha \hat{a}_{\omega'}^{\alpha \dagger} \right) + H.c., \quad (22)$$

where  $P(N)$  is the set of modes of positive (negative) norm. We quantise the GMs by writing the global field  $\mathcal{V}$  in the basis of global *in* modes:

$$\mathcal{V} = \int_0^\infty d\omega' \left( \sum_{\alpha \in P} V_{\omega'}^{in\alpha} \hat{a}_{\omega'}^{in\alpha} + \sum_{\alpha \in N} V_{\omega'}^{in\alpha} \hat{a}_{\omega'}^{in\alpha \dagger} \right) + H.c., \quad (23)$$

or global *out* modes:

$$\mathcal{V} = \int_0^\infty d\omega' \left( \sum_{\alpha \in P} V_{\omega'}^{out\alpha} \hat{a}_{\omega'}^{out\alpha} + \sum_{\alpha \in N} V_{\omega'}^{out\alpha} \hat{a}_{\omega'}^{out\alpha \dagger} \right) + H.c., \quad (24)$$

The expansion (23) for *in* and (24) for *out* modes defines the annihilation and creation operators for the global modes, as well as the transformation between *in* and *out* creation and annihilation operators of the field: the operators  $\hat{a}_{\omega'}^\alpha$  and  $\hat{a}_{\omega'}^{\alpha \dagger}$  are the annihilation and creation operators of the field mode  $\alpha$ . Let  $\hat{A}^{in}$  be the row vector containing all the annihilation and creation operators for positive- and negative-norm global *in* modes, respectively, and  $\hat{A}^{out}$  be the corresponding variable for the *out* modes, then the transformation of operators follows from the definition of  $S$  [21]:

$$\hat{A}^{out} = S \hat{A}^{in}. \quad (25)$$

## 2. Scattering of vacuum states

Having quantised the sets of global *in* and *out* modes, we can use scattering theory to calculate the expectation value in *out* modes of positive or negative norm when *in* modes are in the vacuum state.

Denoting  $\alpha_1$  ( $\bar{\alpha}$ ) as a mode of same (opposite) sign in norm as  $\alpha$ , the incoming state is defined as

$$|0_{in}\rangle = \hat{a}_{\omega'}^{in\alpha_1} |0_{\alpha_1}\rangle \otimes \hat{a}_{\omega'}^{in\bar{\alpha}_1} |0_{\bar{\alpha}_1}\rangle = 0. \quad (26)$$

This state is in the vacuum state defined by the destruction operators associated with the *in* modes of positive and negative norm. The number of particles operator in an *out* mode  $\alpha$  is  $\hat{N}_{\omega'}^\alpha = \hat{a}_{\omega'}^{out\alpha \dagger} \hat{a}_{\omega'}^{out\alpha}$ . It can be written out by identifying the annihilation and creation operators

of the *out* mode from equation (24):

$$\begin{aligned} \hat{N}_{\omega'}^\alpha &= \left( \sum_{\alpha_1} \beta_{\omega'}^{\alpha_1 \alpha^*} \hat{a}_{\omega'}^{\alpha_1 \dagger} + \sum_{\bar{\alpha}_1} \beta_{\omega'}^{\bar{\alpha}_1 \alpha} \hat{a}_{\omega'}^{\bar{\alpha}_1} \right) \times \\ &\quad \left( \sum_{\alpha_1} \beta_{\omega'}^{\alpha_1 \alpha} \hat{a}_{\omega'}^{\alpha_1} + \sum_{\bar{\alpha}_1} \beta_{\omega'}^{\bar{\alpha}_1 \alpha^*} \hat{a}_{\omega'}^{\bar{\alpha}_1 \dagger} \right) \\ &= \sum_{\alpha_1 \alpha'_1} \beta_{\omega'}^{\alpha_1 \alpha^*} \beta_{\omega'}^{\alpha'_1 \alpha} \hat{a}_{\omega'}^{\alpha_1 \dagger} \hat{a}_{\omega'}^{\alpha'_1} + \sum_{\bar{\alpha}_1 \bar{\alpha}'_1} \beta_{\omega'}^{\bar{\alpha}_1 \alpha} \beta_{\omega'}^{\bar{\alpha}'_1 \alpha^*} \hat{a}_{\omega'}^{\bar{\alpha}_1} \hat{a}_{\omega'}^{\bar{\alpha}'_1 \dagger} + \\ &\quad \sum_{\alpha_1 \bar{\alpha}'_1} \beta_{\omega'}^{\alpha_1 \alpha^*} \beta_{\omega'}^{\bar{\alpha}'_1 \alpha} \hat{a}_{\omega'}^{\alpha_1 \dagger} \hat{a}_{\omega'}^{\bar{\alpha}'_1 \dagger} + \sum_{\bar{\alpha}_1 \alpha'_1} \beta_{\omega'}^{\bar{\alpha}_1 \alpha} \beta_{\omega'}^{\alpha'_1 \alpha} \hat{a}_{\omega'}^{\bar{\alpha}_1} \hat{a}_{\omega'}^{\alpha'_1}. \end{aligned} \quad (27)$$

Whence the expectation value for the number of photons in an *out* mode is  $\langle \hat{N}_{\omega'}^\alpha \rangle = \delta\omega' \langle 0_{in} | \hat{N}_{\omega'}^\alpha | 0_{in} \rangle$ . We begin with the second term (all the mixed terms go to zero):

$$\begin{aligned} \langle 0_{in} | \sum_{\bar{\alpha}_1 \bar{\alpha}'_1} \beta_{\omega'}^{\bar{\alpha}_1 \alpha} \beta_{\omega'}^{\bar{\alpha}'_1 \alpha^*} \hat{a}_{\omega'}^{\bar{\alpha}_1} \hat{a}_{\omega'}^{\bar{\alpha}'_1 \dagger} | 0_{in} \rangle &= \\ \delta_\epsilon(0) \sum_{\bar{\alpha}_1 \bar{\alpha}'_1} \beta_{\omega'}^{\bar{\alpha}_1 \alpha} \beta_{\omega'}^{\bar{\alpha}'_1 \alpha^*} \times \left( \langle 0_{in} | \hat{a}_{\omega'}^{\bar{\alpha}_1 \dagger} \hat{a}_{\omega'}^{\bar{\alpha}'_1} | 0_{in} \rangle \right. \\ &\quad \left. + \langle 1|1 \rangle_{in} \delta_{\bar{\alpha}_1 \bar{\alpha}'_1} \right) \\ &= \delta_\epsilon(0) \sum_{\bar{\alpha}_1} |\beta_{\omega'}^{\bar{\alpha}_1 \alpha}|^2, \end{aligned} \quad (28)$$

because the  $\langle 1|1 \rangle_{in}$  term for any mode is nothing but  $\langle 0_{in} | \hat{a}_{\omega'} \hat{a}_{\omega'}^\dagger | 0_{in} \rangle$  and, for the same mode,  $\hat{a} \hat{a}^\dagger - \hat{a}^\dagger \hat{a} = \delta(0)$ , thus

$$\langle 1|1 \rangle_{in} = \langle 0_{in} | \hat{a}^\dagger \hat{a} | 0_{in} \rangle + \langle 0_{in} | \delta(0) | 0_{in} \rangle = \delta(0). \quad (29)$$

Furthermore, by (26), the first term in the parentheses of (28) is zero. Likewise, all the other terms of (27) are zero [38] — therefore,  $\langle \hat{N}_{\omega'}^\alpha \rangle = \sum_{\bar{\alpha}_1} |\beta_{\omega'}^{\bar{\alpha}_1 \alpha}|^2$ . We obtain the flux density of photons  $I_{\omega'}^{\alpha}$  in mode  $\alpha$ , the number of particles per unit time  $\delta\tau$  and bandwidth  $\delta\omega'$  in the moving frame,

$$I_{\omega'}^{\alpha} = \frac{\langle \hat{N}_{\omega'}^\alpha \rangle}{\delta\tau \delta\omega'} = \frac{1}{\delta\tau \delta\omega'} \sum_{\bar{\alpha}} |\beta_{\omega'}^{\bar{\alpha} \alpha}|^2 \quad (30)$$

We have arrived at an interesting result: if *in* Global Modes scatter into *out* Global Modes of opposite norm, light will be emitted from the vacuum at the interface. The amount of light that will be emitted, the photonic flux, can be directly computed from the scattering matrix.

## III. ANALYTICS OF SCATTERING AT THE REFRACTIVE INDEX FRONT

In the previous part of this paper, we arrived at an expression for the scattering matrix, that describes the



conversion of an incoming field to an outgoing field. We now want to derive an analytical formula to calculate the Scattering matrix. For this purpose, we consider a single interface: a step in the refractive index separating two homogeneous regions, as schematically depicted in Fig.2. As we saw in section IIC 1, at each comoving frequency  $\omega'$ , we find 8 mode solutions of the fields equations (7) on either side of the interface. In section IIB we then found that, for a given height of the step (change in the refractive index) there were different, and distinct, comoving-frequency intervals in which 6 or 8 of the mode solutions in either region would be oscillatory modes of the field. When there would be only 6 oscillatory solutions, the remaining two would have complex  $\omega'$  and  $k'$

— that is they would be exponentially growing or decaying waves. Thus, as a function of comoving frequency, we found 5 mode configurations, depending on the number of oscillatory solutions on either side of the interface. In what follows, we shall refer to all mode-solutions (the oscillatory and non-oscillatory solutions alike) as “modes” and only specify their nature where necessary. We called these modes “local modes” (LMs) because they exist in the homogeneous regions on either side of the boundary.

The electromagnetic and polarisation fields and their derivatives in a homogeneous regions are related by Eq.(7). We also established that the electromagnetic field and polarisation fields, and their first spatial derivatives, could be matched at the interface by:

$$\begin{pmatrix} \Pi_A \\ \Pi_{P_1} \\ \Pi_{P_2} \\ \Pi_{P_3} \\ \partial_\zeta \Pi_A \\ \partial_\zeta \Pi_{P_1} \\ \partial_\zeta \Pi_{P_2} \\ \partial_\zeta \Pi_{P_3} \end{pmatrix} = \begin{pmatrix} -i \frac{\omega'}{4\pi c^2} & 0 & 0 & 0 & 0 & 0 & 0 & 0 \\ \frac{\gamma}{c} & -i \frac{\omega' \gamma^2}{\kappa_1 \Omega_1^2} & 0 & 0 & 0 & -\frac{u \gamma^2}{\kappa_1 \Omega_1^2} & 0 & 0 \\ \frac{\gamma}{c} & 0 & -i \frac{\omega' \gamma^2}{\kappa_2 \Omega_2^2} & 0 & 0 & 0 & -\frac{u \gamma^2}{\kappa_2 \Omega_2^2} & 0 \\ \frac{\gamma}{c} & 0 & 0 & -i \frac{\omega' \gamma^2}{\kappa_3 \Omega_3^2} & 0 & 0 & 0 & -\frac{u \gamma^2}{\kappa_3 \Omega_3^2} \\ 0 & 0 & 0 & 0 & -i \frac{\omega'}{4\pi c^2} & 0 & 0 & 0 \\ -i \frac{\omega' \gamma}{cu} & \left( \frac{1}{\kappa_1} - \frac{\omega'^2 \gamma^2}{\kappa_1 \Omega_1^2} \right) \frac{1}{u} & 0 & 0 & 0 & 0 & i \frac{\omega' \gamma^2}{\kappa_1 \Omega_1^2} & 0 \\ -i \frac{\omega' \gamma}{cu} & 0 & \left( \frac{1}{\kappa_2} - \frac{\omega'^2 \gamma^2}{\kappa_2 \Omega_2^2} \right) \frac{1}{u} & 0 & 0 & 0 & 0 & i \frac{\omega' \gamma^2}{\kappa_2 \Omega_2^2} \\ -i \frac{\omega' \gamma}{cu} & 0 & 0 & \left( \frac{1}{\kappa_3} - \frac{\omega'^2 \gamma^2}{\kappa_3 \Omega_3^2} \right) \frac{1}{u} & 0 & 0 & 0 & i \frac{\omega' \gamma^2}{\kappa_3 \Omega_3^2} \end{pmatrix} \begin{pmatrix} A \\ P_1 \\ P_2 \\ P_3 \\ \partial_\zeta A \\ \partial_\zeta P_1 \\ \partial_\zeta P_2 \\ \partial_\zeta P_3 \end{pmatrix}. \quad (31)$$

Henceforth, the last vector of (31) (that contains the fields and their first spatial derivatives) will be called  $\vec{W}$ .

In what follows, we will study the relationship, defined by the scattering matrix, between the incoming and outgoing field for each of the mode configurations (found in section IIB), as functions of the comoving frequency. In doing so, we will derive an analytical formula to calculate the scattering matrix from the matching conditions (31) in all possible mode configurations.

### A. Scattering matrix

In the scattering matrix formalism, the incoming and outgoing fields at the interface are described in terms of global modes (GMs): there are global *in* and global *out* modes, in which light propagates toward and away from the interface, in either of the homogeneous regions, respectively.

#### 1. Reinterpreting the matching conditions

GMs are constructed as linear combinations of LMs: an *out* GM is composed of one LM that has positive (negative) group-velocity in the high (low) refractive-

index region and a collection of 8 LMs that have negative (positive) group-velocity in the high (low) refractive-index region. In the presence of non-oscillatory modes, either the first or one of the later 8 modes may be a non-oscillatory mode. Let us consider an example: over the black-hole-like interval (mode configuration 4, see section IIB), there is a unique *out* GM that allows for light to propagate away from the interface into the low refractive index region (on the right of the interface in Fig.2), *moR*. Its mode decomposition is shown as the spacetime diagram in Fig.5: it is a linear combination of 7 oscillatory LMs, in the right region, that have negative group-velocity, a non-oscillatory LM on the left, and a unique mode that has positive group-velocity in the right region.

The converse to the above delineation leads to constructing *in* GMs, in which light propagates toward the interface. Since there exist 8 LMs on either side of this interface, we find 8 *in* and 8 *out* GMs. These must be arranged in lowering order of laboratory-frame frequency  $\omega$  to allow for a consistent treatment of the matching conditions. Given the relation between the fields, their conjugate momenta and their derivatives, see Eq.(31), the matching conditions are entirely determined by the fields and their derivatives only. Thus we create a matrix of the eight  $\vec{W}$  LM solutions to the dispersion relation,

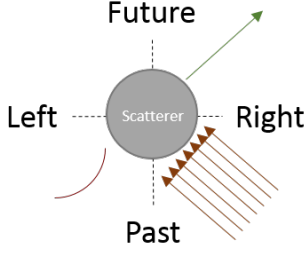


Figure 5. Mode decomposition of the Global Out Mode  $moR$ . In this spacetime diagram, there is a unique mode that propagates away from the scatterer to the right (green arrow). In the past, 7 oscillatory-modes propagate toward the scatterer from the right and there is one non-oscillatory mode on the left of the scatterer.

which we call  $W$ , with

$$W = \left( \vec{W}^{\alpha_1} \vec{W}^{\alpha_2} \dots \vec{W}^{\alpha_8} \right), \quad (32)$$

with  $\alpha_n$ ,  $n = 1, 2, \dots, 8$  the mode number, arranged in decreasing order of laboratory-frame frequency (*i.e.*,  $n = u, uo, mo, \dots, nu$ ). The  $\vec{V}$  and  $\vec{W}$  are related by

$$\vec{V} = \begin{pmatrix} A \\ P_1 \\ P_2 \\ P_3 \\ \Pi_A \\ \Pi_{P_1} \\ \Pi_{P_2} \\ \Pi_{P_3} \end{pmatrix} = \begin{pmatrix} 1 & 0 & 0 & 0 & 0 & 0 & 0 & 0 \\ 0 & 1 & 0 & 0 & 0 & 0 & 0 & 0 \\ 0 & 0 & 1 & 0 & 0 & 0 & 0 & 0 \\ 0 & 0 & 0 & 0 & 1 & 0 & 0 & 0 \\ i\frac{\omega'}{4\pi c^2} & 0 & 0 & 0 & 0 & 0 & 0 & 0 \\ \frac{\gamma}{c} & -i\frac{\omega'\gamma}{\kappa_1\Omega_1^2} & 0 & 0 & 0 & 0 & -\frac{u\gamma^2}{\kappa_1\Omega_1^2} & 0 \\ \frac{\gamma}{c} & 0 & -i\frac{\omega'\gamma}{\kappa_2\Omega_2^2} & 0 & 0 & 0 & 0 & -\frac{u\gamma^2}{\kappa_2\Omega_2^2} \\ \frac{\gamma}{c} & 0 & 0 & 0 & -i\frac{\omega'\gamma}{\kappa_3\Omega_3^2} & 0 & 0 & -\frac{u\gamma^2}{\kappa_3\Omega_3^2} \end{pmatrix} \vec{W}, \quad (33)$$

for a field at frequency  $\omega'$ . We call the matrix in (33)  $\mathcal{U}$ , and remark that  $\text{Det}(\mathcal{U}) = 0$ . In matrices, (33) reads  $V = \mathcal{U}W$ , Note that  $\vec{W}$  and  $\vec{\bar{W}}$  are related by Eq.(6).

The matrix of normalisation factors of the different fields that are connected to the LMs directed toward the interface  $W^{\text{toward}}$  is constructed from the amplitudes of the LMs on the left or the right side of the interface that have negative or positive group-velocity, respectively, as

$$W^{\text{toward}} = W_{L/R} \sigma_{L/R}^{\text{in}}, \quad (34)$$

with, for example on the left side,  $\vec{W}^{\text{toward } \alpha} = W_L \vec{\sigma}_L^{\text{in } \alpha}$ , the linear combination of the amplitudes of LMs that have their group-velocity directed toward the interface. Similarly,

$$W^{\text{away}} = W_{L/R} \sigma_{L/R}^{\text{out}}, \quad (35)$$

wherefrom

$$W^{\text{toward}} = \sigma_{L/R}^{\text{in } T} \sigma_{L/R}^{\text{out } T^{-1}} W^{\text{away } T}, \quad (36)$$

where we have used the relation between the  $V$  and  $W$  matrices, and called on the fact that, them being bases sets, the uniqueness of solutions implies that if they transform at a specific point ( $\zeta = 0$  in (35)), they must do so at any point. In Eq.(36), we have related the amplitude of the incoming field to that of the outgoing field

by means of the scattering matrix  $S$ , with

$$S = \sigma_L^{\text{out}^{-1}} \sigma_L^{\text{in}} = \sigma_R^{\text{out}^{-1}} \sigma_R^{\text{in}}. \quad (37)$$

We have arrived at an expression for the Scattering matrix in terms of the  $\sigma$  matrices, that represent the matching conditions for the Local Modes (LMs) at the interface. From (37), it appears that, in order to calculate the scattering matrix, all that needs being done is to calculate these  $\sigma$  matrices, that is, the Scattering matrix follows directly from the matching conditions. These are  $8 \times 8$  matrices whose components are the coefficient of each LM in the linear expansion of each GM. Thus, they are calculated by using the matching conditions.

## 2. Matching local amplitudes to calculate global ones

In terms of the formalism introduced in the previous paragraph, the fields on the left and on the right of the interface are related by the matching conditions

$$\bar{W}_L \sigma_L^{\text{in } \alpha} = \bar{W}_R \sigma_R^{\text{in } \alpha}, \quad (38)$$

for an *in* field  $\alpha$ , and

$$\bar{W}_L \sigma_L^{\text{out } \alpha} = \bar{W}_R \sigma_R^{\text{out } \alpha}, \quad (39)$$

for an *out* field  $\alpha$ . In Eqs.(38) and (39), the  $\sigma^\alpha$  are  $8 \times 8$  matrices. For every one of these matrices, there are a further 7 constraints to the 8 matching conditions (31)[39]:

- when defining an *in* GM, we set the amplitude of the other LMs that propagate toward the interface 0;
- under wavepacket normalisation, the defining input LM can be regarded as having a finite and tiny bandwidth — *i.e.*, for negative times this LM is the only existing LM and has to be normalised with respect to itself. Thus the defining LM has unit amplitude.

We now proceed to calculating the  $\sigma$  matrices in each mode configuration. Then, each column in Eq.(38) can be written in terms of 8 dimensional column vectors  $\vec{\sigma}^\alpha$

$$\vec{\sigma}_L^{in \alpha} = A \vec{\sigma}_R^{in \alpha}. \quad (40)$$

We define the matrix  $A$  — that is composed of the product amplitudes of LMs on either side of the interface — as

$$A = \bar{W}_L^{-1} \bar{W}_R. \quad (41)$$

It is possible to calculate the  $\sigma$  matrices in terms of the elements of the  $A$  matrix for each mode configuration, and thus the Scattering matrix (by Eq.(37)). The derivation

presented in this section (that revolves around Eq.(37)) is the main analytical result of this paper. In Appendix A we study one mode configuration in detail (further calculations can be found in [18]), and thus explicitly derive the *in* and *out*  $\sigma$  matrices, and the corresponding Scattering matrix.

### 3. Quasi-unitarity of the scattering matrix

The main and usual steps of our calculations are: first we write the A-matrix that gathers the amplitude of the *in*- and *out*-modes on either side of the interface, second we re-arrange the matrix equations to clearly identify the components of the  $\sigma$ -matrices, we then read off the elements of these matrices on the left and the right of the interface and finally use the expression of the scattering matrix as a function of these  $\sigma$ -matrices to explicitly derive it. We found that the scattering matrix is, by construction, a block matrix arranged around a row and a column that account for the non-coupling of oscillatory GMs with non-oscillatory GMs (see Appendix A).

The “normalised” scattering matrix transforms *in* GMs into *out* GMs by Eq.(17). The GMs are normalised by Eq.(21) and, as a result of this normalisation, the scattering matrix is a quasi-unitary matrix. This can be seen by studying the conservation of the Noether current density  $j$  across the interface: the matching conditions across the interface imply that

$$\begin{aligned} -iu(A_L^* \Pi_{A_L^*} + \sum_{i=1}^3 P_{i_L}^* \Pi_{P_{i_L}^*} - \Pi_{A_L} A_L - \sum_{i=1}^3 \Pi_{P_{i_L}} P_{i_L}) &= -iu(A_R^* \Pi_{A_R^*} + \sum_{i=1}^3 P_{i_R}^* \Pi_{P_{i_R}^*} - \Pi_{A_R} A_R - \sum_{i=1}^3 \Pi_{P_{i_R}} P_{i_R}) \\ &\rightarrow j_L = j_R, \end{aligned} \quad (42)$$

where the current and fields on the left (right) of the interface have been ascribed a suffix  $L$  ( $R$ ). Rearranging (42) yields

$$\begin{aligned} V^{out\dagger} g V^{out} &= V^{in\dagger} g V^{in} \\ V^{in\dagger} S^\dagger g S V^{in} &= V^{in\dagger} g V^{in} \\ \rightarrow S^\dagger g S &= g, \end{aligned} \quad (43)$$

where  $g$  is the diagonal matrix with  $N_+$  diagonal elements equal to 1 and  $N_-$  equal to  $-1$ , with  $N_+$  and  $N_-$  the number of GMs of positive and negative norm, respectively. In the present case (8 branches dispersion relation),  $g = \text{diag}(1, 1, 1, 1, 1, -1, -1, -1)$ .

Since the scattering matrix is quasi-unitary, its rows obey the normalisation condition (21), meaning that numerically adding the amplitude squared of all components of a row (multiplied by  $\text{sign}(\omega_\alpha)$ , where  $\omega_\alpha$  is the

laboratory frame frequency and  $\alpha$  is the mode —  $u, uo, mo...$ ) should yield 1. Indeed, by (43),  $S$  is a member of the indefinite unitary group  $U(N_+, N_-)$ . Thus the scattering matrix obeys  $[S^T]^\star g S = g$ , and hence  $S^{-1} = g [S^T]^\star g$ .

Note that ensuring that the Scattering matrix is quasi-unitarity is a standard test that one would wish to perform, for example when computing spectra of emission, or cross-correlation coefficients between modes of emission. We will now present the analytical derivation of these quantities, which will then be numerically computed in the third part of this paper.

## B. Emission spectra and photon flux

We now present two example applications of the Scattering matrix calculated in section III A: first we calculate the density of emission from the vacuum, and then the correlations between modes and across the spectrum of emission.

Optical analogue experiments are different from their fluid-based counterparts (such as BECs [40] or water waves [41–43]) in that the concepts of frames are ‘inverted’: the rest frame of the optical experiment corresponds to the frame of the moving fluid, whereas the moving frame of the optical experiment (that moves together with the RIF) corresponds to the frame in which the potential is static in the fluid experiments. In an optical experiment, measurements are performed in the rest frame of the laboratory, the laboratory frame — where the optical medium and photon counters and all other optical elements and light sources are at rest. Thus, the most interesting set of observables to be computed are the laboratory frame spectral density of emission, and the matrix of cross-correlations across this spectrum. Nevertheless, for the sake of comparison with the fluid-based experiments and theories, we will also present spectra and mode-correlation maps in the moving frame: we hope this will facilitate the dialogue between the communities and clarify the physics at stakes in the optical experiments.

### 1. Photon flux in the moving frame

In the moving frame, the density of emission (per unit time and unit bandwidth), or photon flux, is readily calculated from Eq.(30). A spectrum is thus computed by running through moving frame frequencies  $\omega'$  and summing over the relevant coefficients of the Scattering matrix (37) depending on the *out* Global Mode (GM) under consideration.

### 2. Mode-correlations in the moving frame

The photon number in a mode  $\alpha$  per moving frame bandwidth  $\delta\omega'$  (the reader is referred to Appendix B for a detail of the treatment of the  $\delta$ -function) is

$$\phi_{\omega'}^{\alpha} = \langle 0_{in} | \hat{N}_{\omega'}^{\alpha} | 0_{in} \rangle = \delta_{\epsilon}(0) \sum_{\bar{\alpha}} |S_{\omega'}^{\bar{\alpha}\alpha}|^2, \quad (44)$$

with  $\bar{\alpha}$  a mode of opposite norm-sign as  $\alpha$ . From this second moment in the field operators (see Eq.(25)), it is possible to calculate the covariance in photon number between two *out* GMs  $\alpha_1$  and  $\alpha_2$  as a fourth moment of

the field operators —

$$\begin{aligned} \text{cov}(\phi_{\omega'_1}^{\alpha_1}, \phi_{\omega'_2}^{\alpha_2}) &= \langle \phi_{\omega'_1}^{\alpha_1}, \phi_{\omega'_2}^{\alpha_2} \rangle - \langle \phi_{\omega'_1}^{\alpha_1} \rangle \langle \phi_{\omega'_2}^{\alpha_2} \rangle \\ &= \langle (\phi_{\omega'_1}^{\alpha_1} + \Delta\phi_{\omega'_1}^{\alpha_1}) (\phi_{\omega'_2}^{\alpha_2} + \Delta\phi_{\omega'_2}^{\alpha_2}) \rangle - \langle \phi_{\omega'_1}^{\alpha_1} \rangle \langle \phi_{\omega'_2}^{\alpha_2} \rangle \\ &= \langle \Delta\phi_{\omega'_1}^{\alpha_1} \cdot \Delta\phi_{\omega'_2}^{\alpha_2} \rangle \quad (45) \\ &= \delta_{\epsilon}^2(\omega'_1 - \omega'_2) \sum_{\alpha} \sum_{\bar{\alpha}} |S^{\alpha\alpha_1}|^* |S^{\alpha\alpha_2}| |S^{\bar{\alpha}\alpha_1}| |S^{\bar{\alpha}\alpha_2}|^*, \end{aligned}$$

with  $\alpha, \bar{\alpha}$  a mode of same, opposite, norm-sign as  $\alpha_1$  or  $\alpha_2$ . Similarly, the variance — the squared standard deviation — is

$$\text{var}(\phi_{\omega'_1}^{\alpha_1}) = \text{cov}(\phi_{\omega'_1}^{\alpha_1}, \phi_{\omega'_1}^{\alpha_1}) = \langle \Delta\phi_{\omega'_1}^{\alpha_1 2} \rangle \quad (46)$$

with

$$\langle \Delta\phi_{\omega'_1}^{\alpha_1 2} \rangle = \delta_{\epsilon}^2(0) \sum_{\alpha} \sum_{\bar{\alpha}} |S^{\alpha\alpha_1}|^2 |S^{\bar{\alpha}\alpha_1}|^2. \quad (47)$$

The photon-number Pearson correlation coefficient between two modes  $\alpha_1$  and  $\alpha_2$  is, by definition, the covariance over the product of the standard deviation of each mode —

$$\text{corr}(\phi_{\omega'_1}^{\alpha_1}, \phi_{\omega'_2}^{\alpha_2}) = \frac{\text{cov}(\phi_{\omega'_1}^{\alpha_1}, \phi_{\omega'_2}^{\alpha_2})}{\sqrt{\text{var}(\phi_{\omega'_1}^{\alpha_1}) \text{var}(\phi_{\omega'_2}^{\alpha_2})}}, \quad (48)$$

which, by (45) and (46), is

$$\begin{aligned} \text{corr}(\phi_{\omega'_1}^{\alpha_1}, \phi_{\omega'_2}^{\alpha_2}) &= \frac{\sum_{\alpha} \sum_{\bar{\alpha}} |S^{\alpha\alpha_1}|^* |S^{\bar{\alpha}\alpha_1}|}{\sqrt{\sum_{\alpha} \sum_{\bar{\alpha}} |S^{\alpha\alpha_1}|^2 |S^{\bar{\alpha}\alpha_1}|^2}} \times \\ &\quad \frac{\sum_{\alpha} \sum_{\bar{\alpha}} |S^{\alpha\alpha_2}| |S^{\bar{\alpha}\alpha_2}|^*}{\sqrt{\sum_{\alpha} \sum_{\bar{\alpha}} |S^{\alpha\alpha_2}|^2 |S^{\bar{\alpha}\alpha_2}|^2}} \frac{\delta_{\omega'_1 \omega'_2}}{\delta\omega'}. \quad (49) \end{aligned}$$

Note that the normalisation ensures  $|\text{corr}(\phi_{\omega'_1}^{\alpha_1}, \phi_{\omega'_2}^{\alpha_2})| \leq 1$ .

### 3. Emission in the laboratory frame

We now wish to calculate one of the main two observables of an optical experiment: the density of emission per unit time and unit bandwidth — the real-space spectrum of spontaneous emission from the vacuum at the RIF.

The analytical method presented in section III basically allows for calculating the scattering matrix, *i.e.*, mode conversion in the moving frame. From the scattering matrix (17), we can calculate the flux density of photons in the moving frame, Eq.(30), in a certain *out* GM  $\alpha$  —  $I_{\omega'}^{\alpha}$ . We now want to find which *out* GM  $\alpha$  contributes to the emission for a certain frequency  $\omega$  in the *laboratory* frame. We will then see how to compute the contribution of  $\alpha$  to the total density of emission at  $\omega$ .

Looking back to section IIC 2, we defined an *out* GM as a mode in which light may propagate *away* from the RIF into *either* the high- or low-refractive index region (see also Fig.4). We saw in section IIB that, of

all modes in the medium, only *moR* allows for light to propagate away from the RIF in the low refractive-index region: in the *moving frame*, *moR* has a positive group-velocity. Equivalently, it has a *laboratory frame* group-velocity (positive and) larger than that of the RIF:  $\frac{\partial \omega_{moR}}{\partial k_{moR}} = v_g(\omega_{moR}) > u$ . Modes *noL*, *uoL* and *loL* have a negative *moving frame* group-velocity (light in these modes propagates away from the RIF in the high refractive-index region). Equivalently, their *laboratory frame* group-velocity is lower than that of the RIF. As can be seen on Fig.1, modes *noL* and *uoR* have *positive* laboratory frame group-velocity for  $\omega' > 0$ , whereas *loL* may have *positive and negative* group-velocity in the same conditions. In what follows, we are interested in calculating the spectrum as it can be measured in the laboratory, by detectors positioned on the side of the medium toward which the RIF propagates. Thus, only modes that have a *positive* laboratory-frame group-velocity will contribute to the measured density of emission.

To calculate the density of emission in the laboratory frame (LSD) at frequency  $\omega$ , we simply have to calculate the gradient of the dispersion branch,  $v_g(\omega)$  at  $\omega$  in the high and low refractive-index regions. If  $v_g(\omega)$  is lower (higher) than  $u$  in the high (low) refractive-index region, then the mode  $\alpha$  found at the intersection point of the dispersion relation at  $\omega$  and the contour line

$$\omega' = \gamma(\omega - uk) \quad (50)$$

contributes to the LSD at  $\omega$ . The rate of photon production per unit time and unit bandwidth in the laboratory frame is calculated from the moving-frame flux density by [21, 44]

$$I_\omega^\alpha = \left(1 - \frac{u}{v_g(\omega)}\right) I_{\omega'}^\alpha. \quad (51)$$

The total spectral density at  $\omega$  is then found by adding the contributions of all GMs to the emission [18, 21] —

$$I_\omega = \sum_\alpha I_\omega^\alpha, \quad (52)$$

yielding the spectral density as a function of frequency-bandwidth. The latter converts to the spectral density as a function of wavelength-bandwidth by the factor  $\omega^2/(2\pi c)$ .

#### 4. Spectral correlations in the laboratory frame

The second essential measurement that one would carry in an optical experiment aiming at observing pair production at the optical horizon is the photon-number correlation across spectral intervals. This is the ultimate tool for characterising the quantum state at the output, for it allows to measure entanglement between photons across the spectrum. Here, we present an analytical formula to calculate the spectral correlations as they can be observed in the laboratory frame.

The covariance and variance between the photon-numbers  $N_T$  and  $N_R$  measured at two different wavelengths  $\lambda_T$  and  $\lambda_R$  in the laboratory frame [45] are

$$\text{Cov}(N_T, N_R) = \frac{\sum_\alpha \sum_{\bar{\alpha}} |S^{\alpha\alpha T}|^* |S^{\bar{\alpha}\alpha T}|}{\delta\omega_T |1 - \frac{v}{v_g(\omega_T)}|} \times \frac{\sum_\alpha \sum_{\bar{\alpha}} |S^{\alpha\alpha R}|^* |S^{\bar{\alpha}\alpha R}|}{\delta\omega_R |1 - \frac{v}{v_g(\omega_R)}|}, \quad (53)$$

and

$$\text{Var}(N_T, N_R) = \frac{\sum_\alpha \sum_{\bar{\alpha}} |S^{\alpha\alpha T}|^2 |S^{\bar{\alpha}\alpha T}|^2}{\delta\omega_T |1 - \frac{v}{v_g(\omega_T)}|} \times \frac{\sum_\alpha \sum_{\bar{\alpha}} |S^{\alpha\alpha R}|^2 |S^{\bar{\alpha}\alpha R}|^2}{\delta\omega_R |1 - \frac{v}{v_g(\omega_R)}|}. \quad (54)$$

$\alpha_T$  and  $\alpha_R$  are the modes that contribute to the emission at  $\omega_T$  and  $\omega_R$ , respectively [46].  $\alpha$  ( $\bar{\alpha}$ ) is a mode of same (opposite) norm-sign as  $\alpha_T$  or  $\alpha_R$ . Spectral correlations are thus calculated by

$$\text{Corr}(N_T, N_R) = \frac{\sum_\alpha \sum_{\bar{\alpha}} |S^{\alpha\alpha T}|^* |S^{\bar{\alpha}\alpha T}|}{\sqrt{\sum_\alpha \sum_{\bar{\alpha}} |S^{\alpha\alpha T}|^2 |S^{\bar{\alpha}\alpha T}|^2}} \times \frac{\sum_\alpha \sum_{\bar{\alpha}} |S^{\alpha\alpha R}|^* |S^{\bar{\alpha}\alpha R}|}{\sqrt{\sum_\alpha \sum_{\bar{\alpha}} |S^{\alpha\alpha R}|^2 |S^{\bar{\alpha}\alpha R}|^2}} \delta_{\omega'_T \omega'_R}. \quad (55)$$

The  $\delta$  function ensures that the two laboratory frequency  $\omega_T$  and  $\omega_R$  share the same moving frame frequency — the condition for photons to have been emitted in pairs via the same scattering event at the RIF.

We have now presented a full analytical framework enabling the study of the spontaneous emission of light at a moving refractive index front in a dispersive medium. Our calculation method can be used with any single- and multi-pole dispersion relation that can be cast in the Sellmeier form (8) to analytically calculate the scattering matrix (17), that describes mode mixing at the interface between regions of different refractive index. Once the scattering matrix has been obtained, all observable quantities — flux of emission in the moving and laboratory frames, and photon-number correlation between modes, and across the laboratory-frame spectrum — can be computed. Indeed, as we have demonstrated in this section of the paper, all these quantities depend directly on the amplitude of the elements of the scattering matrix at the (moving-frame) frequency of interest. In the final section of this paper, we will compute these spectra and correlation matrices, and reveal the characteristics of emission at the optical event horizon.

## IV. NUMERICS

The ability to analytically arrive at the S-matrix from the matching conditions of plane-wave solutions to the fields equations in a dispersive medium enables in-depth study of the mixing-process of these modes at the interface between two media of different refractive index. In the remaining of this paper, we will calculate the properties of spontaneous emission of light at a step-like RIF

(as shown on Fig.2). As a case-study, we consider light in bulk fused silica, for which the Sellmeier coefficients are:  $\kappa_{1,2,3} = 0.07142, 0.03246,$  and  $0.05540$  for the elastic constants, and  $\omega_{1,2,3} = 1.90341 \times 10^4 \text{s}^{-1}, 1.62047 \times 10^4 \text{s}^{-1},$  and  $2.7537 \times 10^4 \text{s}^{-1}$  for the resonance frequencies. We will begin with computations in the moving frame, which will allow us to identify the signature of horizon emission in the spectrum, and then proceed to laboratory-frame computations, which are necessary predictions for future experimental investigations.

### A. Horizon emission signature

In [21], we calculated emission spectra into all optical modes for refractive index changes under the step of various amplitude. We found that the spectrum of emission in all modes is highly structured in intervals of black- and white-hole emission, and horizonless emission. In particular, over the horizon intervals, the spectrum has a “shark fin” shape, with a rapid decrease from a peak value to 0 at frequencies corresponding to inversion points in the moving-frame dispersion diagram 3. Here, we perform computations for a step-height  $\delta n = 2 \times 10^{-6}$ , which corresponds to typical refractive index changes that can be created in an experiment [4, 18, 47].

As can be seen on Fig.6, for such  $\delta n$ , the flux density of emission is very low (of the order of  $10^{-10}$  photons per unit bandwidth and unit time), and the emission in the negative-norm mode  $noL$ , and all positive-norm modes is peaked over very narrow frequency intervals. The low-frequency interval corresponds to white-hole emission ( $I_{\omega'}^{noL} \approx 10^{-9}$  photon per unit time and bandwidth), and the large-frequency interval to black-hole emission ( $I_{\omega'}^{noL} \approx 10^{-8}$  photon per unit time and bandwidth). Despite the width of the peaks, their “shark fin” shape remains visible — this really is a signature of horizon-like emission. Over the white-hole interval, emission is strongest in modes  $noL$  (purple line),  $loL$  (orange-dashed line) and  $uoL$  (blue-dotted line) —  $moR$  is not an *out* GM over this interval. Over the black-hole interval, emission is strongest in modes  $noL$  and  $moR$  (green-dot-dashed line).

The flux of  $noL$  is the strongest at all frequencies because, it being the only negative-norm mode of optical frequency, emission into any of  $uoL$ ,  $moR$  and  $loL$  will be accompanied by emission into this mode. In particular, at the horizon, one would expect the pair-wise emission between  $noL$  and one of the positive-norm modes only to be the strongest. This can be assessed by computing the matrix of photon-number correlation between all modes (including non-optical modes) by Eq.(48), as shown on Fig.7.

We observe that negative-norm mode to positive-norm mode correlations dominate at all moving frame frequency. Correlations are strongest between optical modes of positive- and negative-norm at all frequencies, except for  $\omega' > \omega'_{maxR}$ , where the correlations are more

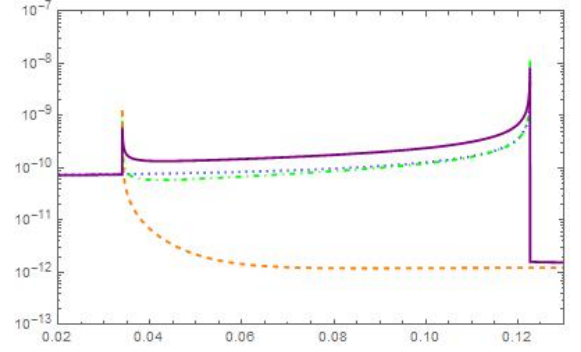


Figure 6. Emission spectra of each optical mode in the moving frame. The fluxes of emission (photons per unit time and bandwidth) of all positive and negative norm modes are plotted together for  $\delta n = 2 \times 10^{-6}$ : emission into mode  $noL$ , purple solid line;  $loL$ , orange dashed line;  $uoL$ , blue dotted line;  $moR$ , green dot-dashed line.

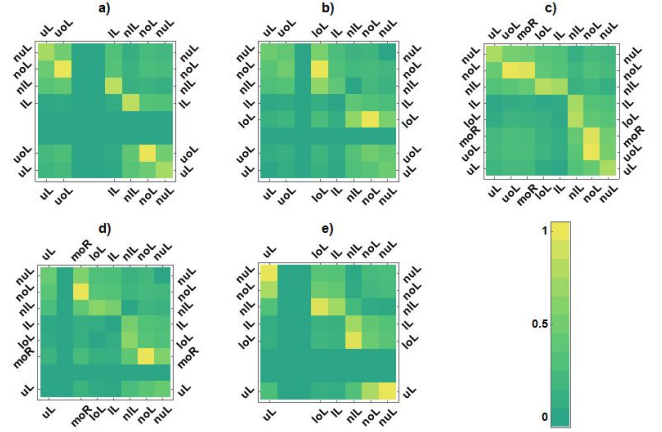


Figure 7. Cross-correlations between mode solutions. Correlations between the 8 *out* GMs in the five frequency intervals is shown for  $\delta n = 2 \times 10^{-6}$ : a)  $\omega' \leq \omega'_{minL}$ ; b)  $\omega'_{minL} < \omega' \leq \omega'_{minR}$  (white-hole interval); c)  $\omega'_{minR} < \omega' \leq \omega'_{maxL}$ ; d)  $\omega'_{maxL} < \omega' \leq \omega'_{maxR}$  (black-hole interval); e)  $\omega' > \omega'_{maxR}$ .

evenly distributed across modes of all branches of the dispersion relation: for example, relatively strong  $nuL$ - $uL$  and  $nlL$ - $loL$  correlations are found. As was anticipated from our study of Fig.6, we see that over the white- and black-hole intervals, the strongest photon-number correlations are between  $noL$  and  $loL$ , and  $noL$  and  $moR$ , respectively. Over the white-hole interval, correlated emission between  $noL$  and  $uoL$  also occurs, although the photon-number correlation coefficient is weak. Furthermore, in the regime of low moving-frame frequency ( $\omega' \leq \omega'_{minL}$ ), strong  $nuL$ - $uL$ ,  $nlL$ - $loL$ , and  $noL$ - $uoL$  correlation coefficients are obtained, with the latter being the strongest. Note that emission between positive-norm modes (such as in between  $uoL$  and  $moR$ ) may be correlated, as can be clearly seen from Fig.6 c), for example.

To summarise, we have found that, over intervals for which the mode-mixing at the boundary is analogous to

(white- or black-hole) horizon physics, the flux of spontaneous emission from the vacuum is stronger than otherwise by at least an order of magnitude. Moreover, the spectrum has a characteristic “shark fin” shape which is robust against  $\delta n$  amplitude changes [21]. Over the analogue white- and black-hole intervals, (quasi) pair-wise emission at optical frequencies dominates, as is proven by the strong negative-norm mode to positive-norm mode photon-number correlation coefficient obtained. Clearly, these are signature effects of horizon physics in dispersive (optical) media that one would want to observe in an experiment.

### B. Horizon physics in the laboratory frame

The spectral properties we have identified in the above section would be observed in the frame co-moving with the RIF in the medium. In an experiment, the detectors are sitting in the laboratory, the rest frame of the medium — the laboratory frame. We will now show that the signature effects of horizon physics — enhanced emission, spectral shape and correlations — are visible in the result of laboratory frame computations.

We begin with a computation of the laboratory frame spectral density (52) for  $\delta n = 2 \times 10^{-6}$ , shown on Fig.8. As its moving-frame counterpart, the spectrum is highly structured into intervals with white- and black-hole emission, and horizonless emission. Emission is strongest over analogue white- and black-hole intervals: from short to long wavelength, we first encounter a peak at 209.8nm, which corresponds to black-hole emission into *noL* — this peak bears some features of the “shark fin”. The strongest peak is found at 227nm, where white-hole emission into *noL* occurs. The spectrum then generally decreases until  $\lambda_{vm} = 396.3$ nm. At this wavelength, the edges of the black-hole interval for *uoL* and *moR* (at short and long wavelength, respectively) overlap. The LSD is minimal (about 5 orders of magnitude lower than the general LSD background) at  $\lambda_{vm} = 396.3$ nm. This feature is the same as that observed at the extrema of the white- and black-hole intervals in the moving frame (see Fig.6 in section IV A) [48]. We finally observe a peak between  $3\lambda_{vm}$  and 398nm, the black-hole interval for *moR*. This peak clearly exhibits the signature “shark fin” structure of horizon emission. Beyond this peak, the LSD monotonously decreases [49].

The various spectral features we have identified have very narrow linewidth: of the order of 1nm or less in the UV, and of 2nm in the visible. They also are neatly peaked above the general LSD background, with densities above  $10^{13}$  photon per second and per meter in the UV (on top of a background of maximally  $10^{12}$ ) and above  $10^{11}$  photon per second and meter for the black-hole emission into *moR* between 396 and 398nm (above a generally decreasing background of maximally half this emission spectral density). These horizon-emission peaks thus represent targets of choice for optical experiments.

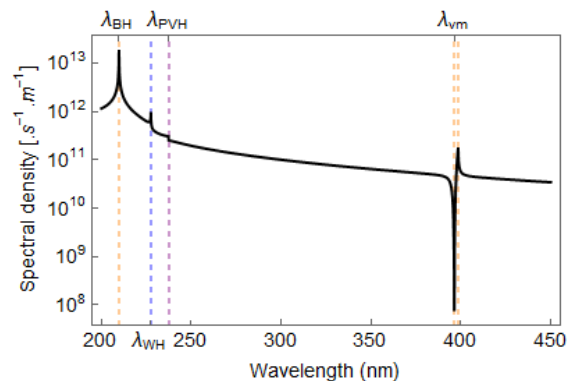


Figure 8. Spectral density of emission in the laboratory frame. At each wavelength the total spectral flux density, the number of photons emitted per unit time and unit bandwidth, is the sum of contributions from all modes, as per Eq.(52). The spectrum is computed for a RIF of height  $\delta n = 2 \times 10^{-6}$  moving at velocity  $u = \frac{2}{3}c$  in bulk fused silica. Horizon-like intervals of emission are found at dashed lines: 209.8nm, black-hole for *noL* (orange-dashed line); 227nm, white-hole for *noL* (blue-dashed line); and  $\lambda_{vm} = 396.3$ nm, black-hole for *moR* (orange dashed-lines). There is a phase velocity horizon at  $\lambda_{pvh} = 237$ nm (purple-dashed line).

In addition to measuring these peaks, measuring their photon-number correlation would be the ultimate proof of their vacuum-fluctuation origin.

In Fig.9, we compute the photon-number Pearson correlation coefficient (55) across the spectrum of laboratory frame emission Fig.8. We see that these coefficients are generally zero, except on the diagonal of the matrix, and over two parabola, one at short-to-long wavelengths and one at long-to-long wavelengths. The diagonal corresponds to self-correlations, and we decided to calculate the single frequency noise

$$\text{Corr}(\lambda_T, \lambda_R) = 1 - \frac{N_\lambda}{\langle \Delta N_\lambda^2 \rangle}, \quad \lambda_T = \lambda_R = \lambda \quad (56)$$

with  $N_\lambda$  the photon number at wavelength  $\lambda$  and  $\langle \Delta N_\lambda^2 \rangle$  the variance in this photon number. The long-to-long wavelengths parabola stems to correlations between *uoL* and *moR* over wavelength intervals corresponding to the “middle” *moving-frame* frequency interval (*i.e.*,  $\omega'_{minR} < \omega' \leq \omega'_{maxL}$ ). Both of these modes have positive norm, and thus the correlation coefficient, although it is not zero, is very weak.

The short-to-long wavelength parabola stems from correlation between the negative-norm mode *noL* (which emits in the UV) and the positive-norm modes *uoL* (for wavelengths between 237 and 396nm) and *moR* (for wavelengths longer than 396nm). The strength of the correlation coefficients along the parabola gradually decreases as the wavelength of *noL* decreases and the wavelength of *uoL* and subsequently *moR* increases. Note that the coefficient is close to 1 as the diagonal is approached, and does not drop below 0.5 along the parabola.

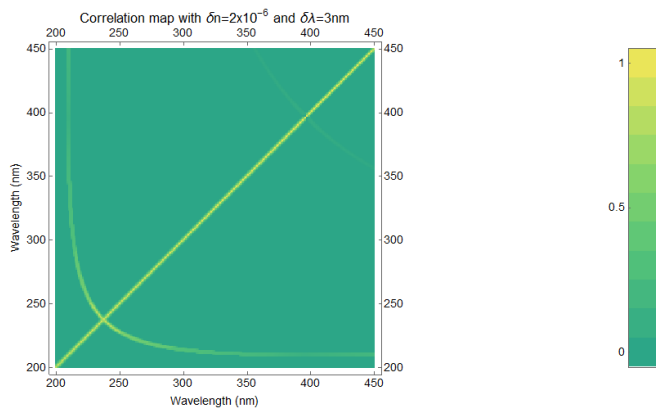


Figure 9. Matrix of cross-correlations (55) across the laboratory-frame spectrum of spontaneous emission 8 for a RIF of height  $\delta n = 2 \times 10^{-6}$  moving at velocity  $u = \frac{2}{3}c$  in bulk fused silica.

Interestingly, the strong correlation features observed in the moving frame are not seen in the laboratory frame computation — although the calculation of the correlation coefficient is the same beyond a trivial multiplication factor. This is because the grid size of our computation is too coarse to let the very narrow spectral features of horizon emission (see the discussion of Fig.8) emerge. We could engineer the numerical computation to show these features, in which case strong correlation coefficients where pair-wise emission at the horizon (*noL-uoL* at the white-hole, and *noL-moR* at the black-hole) occurs, but this is not what could actually be seen in an experiment. Indeed, experimental abilities, in terms of spectral resolution in particular, is too limited for such an engineering of the measured correlation matrix to be feasible. Instead, it is important to remark that wavelength-correlations dominate: what Fig.9 shows is that, in the laboratory frame, strong correlations will be observed among wavelength-pairs across which pair-wise emission is distributed (irrespective of the relative strength of emission). This is a characteristic feature of spontaneous emission at a moving RIF that could be observed in an experiment.

## V. DISCUSSION AND CONCLUSION

### A. Significance of the results

The analytical method presented in this paper is a significant step forward in the vivid field of optical horizon physics. It allows for readily calculating the scattering

matrix in all configurations of refractive index change (height of the step-like RIF  $\delta n$ ) and at all frequencies — including conditions in which the configuration of modes at the interface is analogous to that at black- and white-hole horizons. Furthermore, we have developed a whole analytical framework based on this method that enables rapid computation of real- and frequency-space characteristics of spontaneous emission at the interface between two media homogeneous in their refractive index.

The set of numerical computations presented in the last part of this paper provides all the essential information necessary to carry an optical experiment aimed at observing the spontaneous emission of light at the horizon: the laboratory-frame wavelength and emission strength, as well as the spectral correlations, of pair-wise emission. The moving-frame computations will also facilitate conversation between the fluid-based and optics-based analogue-horizon communities (for whom the concepts of moving and rest frame are inverted). Thus, these calculations represent the full set of observables necessary to the study of horizon physics in dispersive media.

### B. Use and extension of the method

It would be interesting to compute such a spectrum as Fig.8 for a different geometry of the RIF, for example a more realistic pulse shape such as a hyperbolic secant squared, to assess which of the numerous features displayed in Fig.8 are conserved. Efforts in this direction have been pursued in recent publications, see for example [13, 27, 28], in which analytical or numerical calculations in the moving frame were carried for smooth RIF geometries — but no spectrum in the laboratory frame, or even pulse-like geometries (with asymptotically-flat, low-refractive-index, regions on either side of a symmetric bell-shaped RIF) were computed [50].

In the search for spontaneous emission from an optical setup, the study of the simple geometry of the step-like RIF has proven extremely informative in that it has allowed for:

1. clearly establishing the matching conditions between the fields on either side of the interface;
2. clearly identifying the various contributors to emission in positive- and negative-norm modes;
3. creating an analytical method to describe the scattering of an incoming field into outgoing fields without approximations — indeed, in contrast with the above-mentioned publications, we consider exact solutions to the fields equations in asymptotically flat regions around the interface, and do not resort to the JWKB approximation, for example;
4. discovering signature features of event horizon physics in dispersive media, such as the increase in the photon flux over horizon-intervals and the shape of this increase;



5. computing the first spectrum of light spontaneously emitted from the vacuum as it can be observed in the laboratory frame for realistic RIF heights  $\delta n$  (see also [21]);
6. calculating and computing the correlation coefficient between modes (in the moving frame) and across the spectrum of emission (in the laboratory frame), and thus unequivocally establishing the pair-wise character of emission at a moving RIF in a dispersive medium.

The method presented in part III of this paper can be generalised to study more complicated RIF geometries (such as a pulse), which would allow to calculate the scattering matrix describing wave-mixing at such a RIF, and the resulting spectra and correlations. This objective is brought closer to reach by the present work, and shall be the subject of future publication.

### C. Conclusions

The present paper is part of a large and growing body of work on the laboratory observation of spontaneous emission at analogue horizons, an effect akin to Hawking radiation. The latter hints at a connection between Quantum physics and General Relativity, and is widely seen as a pathway to new Physics, beyond these two fundamental theories. Therefore, a lot of effort is going into asserting its existence and observing it. This can unfortunately not be done in astrophysics because of the nK temperature of the flux from black holes. It is however possible to reproduce certain features of General Relativity that one normally thinks of as intrinsically aspects of gravity in condensed matter setups. This was demonstrated in 1981 by Unruh, who showed that both classical and semi-classical features of General Relativity (such as

horizons and Hawking radiation) can, in the context of acoustic manifolds, be seen to be rather generic features of field theories in curved spacetime [3].

In this scheme, our paper considers the problem of calculating the mixing of modes of positive- and negative-norm at the horizon in dispersive, optical media. We present an analytical method for calculating the properties of spontaneous emission resulting from this mode-mixing process that is based on a theoretical framework [20] that uses the Hopfield model [23–25] to describe light-matter interactions. Our method allows for deriving the scattering matrix — that describes the mixing of modes at a moving, step-like Refractive Index Front (RIF) — in all RIF height ( $\delta n$ , the variation in refractive index under the step) and co-moving frequency configurations. Under certain conditions, this RIF may act as a black- or white-hole horizon to modes of the field. The RIF also acts as a horizonless emitter [21], and our method allows for readily calculating the scattering matrix in all cases. The ability to obtain the scattering matrix analytically enables further use of the method: for example, it allows for calculating the photon flux and spectral correlation of spontaneous emission at the RIF, and yields fast numerical computation of these quantities. Our work provides theorists with an analytical method based on a widely-used theoretical framework, and experimentalists with a complete set of observables necessary to establish the vacuum-fluctuations-at-the-horizon origin of their spectra.

### ACKNOWLEDGMENTS

The authors are thankful to Vyome Singh and Maya Petkova for insightful conversations. This work was funded by EPSRC via Grant No. EP/L505079/1.

- 
- [1] S. W. Hawking, *Nature* **248**, 30 (1974).
  - [2] S. W. Hawking, *Communications In Mathematical Physics* **43**, 199 (1975).
  - [3] W. G. Unruh, *Physical Review Letters* **46**, 1351 (1981).
  - [4] T. G. Philbin, C. Kuklewicz, S. Robertson, S. Hill, F. Konig, and U. Leonhardt, *Science* **319**, 1367 (2008).
  - [5] J. S. H. P. Lisle, *ArXiv* (2006).
  - [6] W. G. Unruh, *Phys. Rev. D* **51**, 2827 (1995).
  - [7] I. Carusotto, S. Fagnocchi, A. Recati, R. Balbinot, and A. Fabbri, *New Journal of Physics* **10**, 103001 (2008).
  - [8] S. Corley, *Phys. Rev. D* **57**, 6280 (1998).
  - [9] U. Leonhardt and S. Robertson, *New Journal of Physics* **14**, 053003 (2012).
  - [10] J. Macher and R. Parentani, *Physical Review D* **79** (2009), 10.1103/PhysRevD.79.124008.
  - [11] S. Corley and T. Jacobson, *Phys. Rev. D* **54**, 1568 (1996).
  - [12] S. Robertson, *Hawking radiation in dispersive media*, Ph.D. thesis, University of St Andrews, St Andrews (2011).
  - [13] S. Robertson, *Physical Review E* **90** (2014), 10.1103/PhysRevE.90.053303.
  - [14] S. Robertson and U. Leonhardt, *Physical Review E* **90** (2014), 10.1103/PhysRevE.90.053302.
  - [15] S. Corley, *Phys. Rev. D* **55**, 6155 (1997).
  - [16] A. Recati, N. Pavloff, and I. Carusotto, *Phys. Rev. A* **80**, 043603 (2009).
  - [17] S. Finazzi and R. Parentani, *Physical Review D* **85** (2012), 10.1103/PhysRevD.85.124027.
  - [18] M. J. Jacquet, *Negative frequency at the horizon: scattering of light at a refractive index front*, Ph.D. thesis, University of St Andrews, St Andrews (2017).
  - [19] In [4, 47, 51] or [18], the amplitude of refractive index change is maximally of the order of  $\delta n = 10^{-6}$ , which corresponds to a difference of less than 0.1% in the dielectric constant across the RIF.
  - [20] S. Finazzi and I. Carusotto, *Physical Review A* **87** (2013),

- 10.1103/PhysRevA.87.023803.
- [21] M. Jacquet and F. König, Physical Review A **92** (2015), 10.1103/PhysRevA.92.023851.
- [22] Note that the method is rather general and could be adapted to consider materials with less than three resonances, such as diamond (which has only one resonance). In doing so, one could analytically and numerically obtain spectra for the studies [26–28].
- [23] J. J. Hopfield, Physical Review **112**, 1555 (1958).
- [24] U. Fano, Physical Review **103**, 1202 (1956).
- [25] R. Schützhold, G. Plunien, and G. Soff, Phys. Rev. Lett. **88**, 061101 (2002).
- [26] S. Finazzi and I. Carusotto, Physical Review A **89** (2014), 10.1103/PhysRevA.89.053807.
- [27] F. Belgiorno, S. Cacciatori, and F. Dalla Piazza, Physical Review D **91** (2015), 10.1103/PhysRevD.91.124063.
- [28] M. F. Linder, R. Schützhold, and W. G. Unruh, Physical Review D **93** (2016), 10.1103/PhysRevD.93.104010.
- [29] The model does not account for the dispersion changes due to the finiteness of the intersites distance.
- [30] C. Cohen-Tannoudji, J. Dupont-Roc, and G. Grynberg, *Photons and atoms: introduction to quantum electrodynamics*, nachdr. ed., Physics textbook (Wiley, Weinheim, 2004) oCLC: 254806943.
- [31] The magnitude of the refractive index change giving rise to the various mode configurations depends on the medium properties. For the sake of the argument presented in this section it suffices to identify three categories of refractive index change: small, medium, and large — exact numbers will be provided by the numerical analysis carried in the final section of this paper.
- [32] B. Huttner, J. J. Baumberg, and S. M. Barnett, Europhysics Letters (EPL) **16**, 177 (1991).
- [33] B. Huttner and S. M. Barnett, Europhysics Letters (EPL) **18**, 487 (1992).
- [34] R. Matloob, R. Loudon, S. M. Barnett, and J. Jeffers, Physical Review A **52**, 4823 (1995).
- [35] S. M. Barnett, R. Matloob, and R. Loudon, Journal of Modern Optics **42**, 1165 (1995).
- [36] D. J. Santos and R. Loudon, Physical Review A **52**, 1538 (1995).
- [37] S. M. Barnett, B. Huttner, and R. Loudon, Physical Review Letters **68**, 3698 (1992).
- [38] The commutation of the *out* modes on the *in* modes gives zero and all the mixed terms go to zero.
- [39] For the unphysical (exponentially growing) mode, this is different: it is defined as the unphysical mode *only* on one side. This GM serves as *in* — and identically as *out* — mode. Hence unphysical GMs scatter into themselves, by definition.
- [40] J. Steinhauer, Nature Physics **12**, 959 (2016).
- [41] G. Rousseaux, C. Mathis, P. Massa, T. G. Philbin, and U. Leonhardt, New Journal of Physics **10**, 053015 (2008).
- [42] S. Weinfurter, E. W. Tedford, M. C. J. Penrice, W. G. Unruh, and G. A. Lawrence, Physical Review Letters **106** (2011), 10.1103/PhysRevLett.106.021302.
- [43] L.-P. Euvé, F. Michel, R. Parentani, T. G. Philbin, and G. Rousseaux, Phys. Rev. Lett. **117**, 121301 (2016).
- [44] I. Carusotto and C. Ciuti, Reviews of Modern Physics **85**, 299 (2013).
- [45] The photon number is related to the LSD by  $N_T = I_\omega \delta\omega \delta t$ .
- [46] Note that there may be more than one mode that contributes to the emission at any  $\omega$ , in which case (53) has to be amended to account for this. This is fully implemented in our numerical calculations.
- [47] A. Choudhary and F. König, Optics Express **20**, 5538 (2012).
- [48] Note that at the extrema of the horizon-like intervals, the emission drops to zero as the group-velocity of the *out* GM becomes zero in the moving frame: light cannot escape from the RIF in a mode that is velocity-matched with it.
- [49] Until the horizon intervals for *loL*, which will be at extremely long wavelengths in the Infra-Red [18, 21] and are not interesting for the sake of this study.
- [50] In [52], the method [13, 14] was applied to an unrealistic situation: a spectrum of spontaneous emission from an extremely short pulse, of  $T_0 = 2\text{fs}$ , that is a 1.25 cycle-long pulse (for  $\lambda_c = 800\text{nm}$ ) in the laboratory frame. Such a short pulse can probably not be created in an actual experiment, propagate through a dispersive medium or not contaminate the signal frequencies with its own bandwidth.
- [51] D. Faccio, S. Cacciatori, V. Gorini, V. G. Sala, A. Averchi, A. Lotti, M. Kolesik, and J. V. Moloney, EPL (Europhysics Letters) **89**, 34004 (2010).
- [52] D. Bermudez and U. Leonhardt, Physical Review A **93** (2016), 10.1103/PhysRevA.93.053820.

## Appendix A: Scattering matrix from the matching conditions

In this appendix we explicitly derive the Scattering matrix in mode configuration 3, which corresponds to a moving frame interval over which there are 8 oscillatory mode-solutions on either side of the interface (see section IIB). We arrange both the global and local modes in decreasing order of comoving frame wavenumber  $k'$ : *u uo mo lo l nl no nu*. We use matrices to relate GMs (columns) to LMs (rows), whereby the first column (row) of a matrix describes the GM (LM) *u*, the second *uo* and so on. In mode configuration 3, there are 8 oscillating LMs on either side of the interface. Then, (40) reads

$$\begin{pmatrix} 1 & 0 & 0 & 0 & 0 & 0 & 0 & 0 \\ 0 & 0 & 1 & 0 & 0 & 0 & 0 & 0 \\ \vdots & \vdots & \vdots & \vdots & \vdots & \vdots & \vdots & \vdots \\ 0 & 0 & 1 & 0 & 0 & 0 & 0 & 0 \end{pmatrix} = A \begin{pmatrix} 1 & 0 & 0 & 0 & 0 & 0 & 0 & 0 \\ 0 & 1 & 0 & 0 & 0 & 0 & 0 & 0 \\ \vdots & \vdots & \vdots & \vdots & \vdots & \vdots & \vdots & \vdots \\ 0 & 0 & 0 & 1 & 0 & 0 & 0 & 0 \\ 0 & 0 & 0 & 0 & 1 & 0 & 0 & 0 \\ 0 & 0 & 0 & 0 & 0 & 1 & 0 & 0 \\ 0 & 0 & 0 & 0 & 0 & 0 & 1 & 0 \\ 0 & 0 & 0 & 0 & 0 & 0 & 0 & 1 \end{pmatrix} \quad (\text{A1})$$

There are 64 unknowns, materialised as “empty” components of the matrices. In order to find the  $\sigma^{in}$  matrix in this mode configuration, we proceed to re-arranging (A1):

$$\begin{pmatrix} \vec{\sigma}_{L1}^T \\ \vec{\sigma}_{L2}^T \\ 0 \\ \vec{\sigma}_{L4}^T \\ \vec{\sigma}_{L5}^T \\ \vec{\sigma}_{L6}^T \\ \vec{\sigma}_{L7}^T \\ \vec{\sigma}_{L8}^T \end{pmatrix} - \begin{pmatrix} A_{13} \vec{\sigma}_{R3}^T \\ A_{23} \vec{\sigma}_{R3}^T \\ A_{33} \vec{\sigma}_{R3}^T \\ A_{43} \vec{\sigma}_{R3}^T \\ A_{53} \vec{\sigma}_{R3}^T \\ A_{63} \vec{\sigma}_{R3}^T \\ A_{73} \vec{\sigma}_{R3}^T \\ A_{83} \vec{\sigma}_{R3}^T \end{pmatrix} = \begin{pmatrix} A_{11} & A_{12} & 0 & A_{14} & A_{15} & A_{16} & A_{17} & A_{18} \\ A_{21} & A_{22} & 0 & A_{24} & A_{25} & A_{26} & A_{27} & A_{28} \\ A_{31} & A_{32} & -1 & A_{34} & A_{35} & A_{36} & A_{37} & A_{38} \\ A_{41} & A_{42} & 0 & A_{44} & A_{45} & A_{46} & A_{47} & A_{48} \\ A_{51} & A_{52} & 0 & A_{54} & A_{55} & A_{56} & A_{57} & A_{58} \\ A_{61} & A_{62} & 0 & A_{64} & A_{65} & A_{66} & A_{67} & A_{68} \\ A_{71} & A_{72} & 0 & A_{74} & A_{75} & A_{76} & A_{77} & A_{78} \\ A_{81} & A_{82} & 0 & A_{84} & A_{85} & A_{86} & A_{87} & A_{88} \end{pmatrix} = \tag{A2}$$

$$\left[ \begin{pmatrix} 1 & 0 & 0 & 0 & 0 & 0 & 0 & 0 \\ 0 & 1 & 0 & 0 & 0 & 0 & 0 & 0 \\ 0 & 0 & 0 & 0 & 0 & 0 & 0 & 0 \\ 0 & 0 & 0 & 1 & 0 & 0 & 0 & 0 \\ 0 & 0 & 0 & 0 & 1 & 0 & 0 & 0 \\ 0 & 0 & 0 & 0 & 0 & 1 & 0 & 0 \\ 0 & 0 & 0 & 0 & 0 & 0 & 1 & 0 \\ 0 & 0 & 0 & 0 & 0 & 0 & 0 & 1 \end{pmatrix} - (\vec{0} \ \vec{0} \ \vec{A}_3 \ \vec{0} \ \vec{0} \ \vec{0} \ \vec{0} \ \vec{0}) \right] \times \begin{pmatrix} \vec{\sigma}_{L1}^T \\ \vec{\sigma}_{L2}^T \\ \vec{\sigma}_{R3}^T \\ \vec{\sigma}_{L4}^T \\ \vec{\sigma}_{L5}^T \\ \vec{\sigma}_{L6}^T \\ \vec{\sigma}_{L7}^T \\ \vec{\sigma}_{L8}^T \end{pmatrix}.$$

We obtain

$$\sigma^{in} = \begin{pmatrix} A_{11} - \frac{A_{13}A_{31}}{A_{33}} & A_{12} - \frac{A_{13}A_{32}}{A_{33}} & \frac{A_{13}}{A_{33}} & A_{14} - \frac{A_{13}A_{34}}{A_{33}} & - & - & - & - \\ A_{21} - \frac{A_{23}A_{31}}{A_{33}} & A_{22} - \frac{A_{23}A_{32}}{A_{33}} & \frac{A_{23}}{A_{33}} & A_{24} - \frac{A_{23}A_{34}}{A_{33}} & - & - & - & - \\ -\frac{A_{31}}{A_{33}} & -\frac{A_{32}}{A_{33}} & \frac{1}{A_{33}} & -\frac{A_{34}}{A_{33}} & - & - & - & - \\ A_{41} - \frac{A_{43}A_{31}}{A_{33}} & A_{42} - \frac{A_{43}A_{32}}{A_{33}} & \frac{A_{43}}{A_{33}} & A_{44} - \frac{A_{43}A_{34}}{A_{33}} & - & - & - & - \\ A_{81} - \frac{A_{83}A_{31}}{A_{33}} & A_{82} - \frac{A_{83}A_{32}}{A_{33}} & \frac{A_{83}}{A_{33}} & A_{84} - \frac{A_{83}A_{34}}{A_{33}} & - & - & - & - \end{pmatrix}. \tag{A3}$$

For the *out* modes, (A1) is

$$\begin{pmatrix} 1 & 0 & 0 & 0 & 0 & 0 & 0 & 0 \\ 0 & 1 & 0 & 0 & 0 & 0 & 0 & 0 \\ 0 & 0 & 0 & 1 & 0 & 0 & 0 & 0 \\ 0 & 0 & 0 & 0 & 1 & 0 & 0 & 0 \\ 0 & 0 & 0 & 0 & 0 & 1 & 0 & 0 \\ 0 & 0 & 0 & 0 & 0 & 0 & 1 & 0 \\ 0 & 0 & 0 & 0 & 0 & 0 & 0 & 1 \end{pmatrix} = A \begin{pmatrix} 0 & 0 & 1 & 0 & 0 & 0 & 0 & 0 \end{pmatrix}, \tag{A4}$$

and similar algebra to the above (exchange  $A$  and  $A^{-1}$ ) leads to the conclusion that

$$\sigma_R^{outT} = \sigma_L^{inT}, \tag{A5}$$

that is, one can be calculated from the other by using either  $A$  or its inverse.

From the above  $\sigma^{in/out}$  matrices, we identify the  $\sigma_{L/R}^{in/out}$  matrices:

$$\begin{aligned}
\sigma_L^{in} &= \begin{pmatrix} A_{11} - \frac{A_{13}A_{31}}{A_{33}} & A_{12} - \frac{A_{13}A_{32}}{A_{33}} & \frac{A_{13}}{A_{33}} & A_{14} - \frac{A_{13}A_{34}}{A_{33}} & - & - & - & - \\ A_{21} - \frac{A_{23}A_{31}}{A_{33}} & A_{22} - \frac{A_{23}A_{32}}{A_{33}} & \frac{A_{23}}{A_{33}} & A_{24} - \frac{A_{23}A_{34}}{A_{33}} & - & - & - & - \\ 0 & 0 & 1 & 0 & 0 & 0 & 0 & 0 \\ A_{41} - \frac{A_{43}A_{31}}{A_{33}} & A_{42} - \frac{A_{43}A_{32}}{A_{33}} & \frac{A_{43}}{A_{33}} & A_{44} - \frac{A_{43}A_{34}}{A_{33}} & - & - & - & - \\ \vdots & \vdots & \vdots & \vdots & \vdots & \vdots & \vdots & \vdots \\ A_{81} - \frac{A_{83}A_{31}}{A_{33}} & A_{82} - \frac{A_{83}A_{32}}{A_{33}} & \frac{A_{83}}{A_{33}} & A_{84} - \frac{A_{83}A_{34}}{A_{33}} & - & - & - & - \end{pmatrix} \\
\sigma_R^{in} &= \begin{pmatrix} 1 & 0 & 0 & 0 & 0 & 0 & 0 & 0 \\ 0 & 1 & 0 & 0 & 0 & 0 & 0 & 0 \\ -\frac{A_{31}}{A_{33}} & -\frac{A_{32}}{A_{33}} & \frac{1}{A_{33}} & -\frac{A_{34}}{A_{33}} & -\frac{A_{35}}{A_{33}} & -\frac{A_{36}}{A_{33}} & -\frac{A_{37}}{A_{33}} & -\frac{A_{38}}{A_{33}} \\ 0 & 0 & 0 & 1 & 0 & 0 & 0 & 0 \\ 0 & 0 & 0 & 0 & 1 & 0 & 0 & 0 \\ 0 & 0 & 0 & 0 & 0 & 1 & 0 & 0 \\ 0 & 0 & 0 & 0 & 0 & 0 & 1 & 0 \\ 0 & 0 & 0 & 0 & 0 & 0 & 0 & 1 \end{pmatrix} \\
\sigma_L^{out} &= \begin{pmatrix} 1 & 0 & 0 & 0 & 0 & 0 & 0 & 0 \\ 0 & 1 & 0 & 0 & 0 & 0 & 0 & 0 \\ -\frac{A_{31}^{-1}}{A_{33}} & -\frac{A_{32}^{-1}}{A_{33}} & \frac{1}{A_{33}} & -\frac{A_{34}^{-1}}{A_{33}} & -\frac{A_{35}^{-1}}{A_{33}} & -\frac{A_{36}^{-1}}{A_{33}} & -\frac{A_{37}^{-1}}{A_{33}} & -\frac{A_{38}^{-1}}{A_{33}} \\ 0 & 0 & 0 & 1 & 0 & 0 & 0 & 0 \\ 0 & 0 & 0 & 0 & 1 & 0 & 0 & 0 \\ 0 & 0 & 0 & 0 & 0 & 1 & 0 & 0 \\ 0 & 0 & 0 & 0 & 0 & 0 & 1 & 0 \\ 0 & 0 & 0 & 0 & 0 & 0 & 0 & 1 \end{pmatrix} \\
\sigma_R^{out} &= \begin{pmatrix} A_{11}^{-1} - \frac{A_{13}^{-1}A_{31}^{-1}}{A_{33}} & A_{12}^{-1} - \frac{A_{13}^{-1}A_{32}^{-1}}{A_{33}} & \frac{A_{13}^{-1}}{A_{33}} & A_{14}^{-1} - \frac{A_{13}^{-1}A_{34}^{-1}}{A_{33}} & - & - & - & - \\ A_{21}^{-1} - \frac{A_{23}^{-1}A_{31}^{-1}}{A_{33}} & A_{22}^{-1} - \frac{A_{23}^{-1}A_{32}^{-1}}{A_{33}} & \frac{A_{23}^{-1}}{A_{33}} & A_{24}^{-1} - \frac{A_{23}^{-1}A_{34}^{-1}}{A_{33}} & - & - & - & - \\ 0 & 0 & 1 & 0 & 0 & 0 & 0 & 0 \\ A_{41}^{-1} - \frac{A_{43}^{-1}A_{31}^{-1}}{A_{33}} & A_{42}^{-1} - \frac{A_{43}^{-1}A_{32}^{-1}}{A_{33}} & \frac{A_{43}^{-1}}{A_{33}} & A_{44}^{-1} - \frac{A_{43}^{-1}A_{34}^{-1}}{A_{33}} & - & - & - & - \\ \vdots & \vdots & \vdots & \vdots & \vdots & \vdots & \vdots & \vdots \\ A_{81}^{-1} - \frac{A_{83}^{-1}A_{31}^{-1}}{A_{33}} & A_{82}^{-1} - \frac{A_{83}^{-1}A_{32}^{-1}}{A_{33}} & \frac{A_{83}^{-1}}{A_{33}} & A_{84}^{-1} - \frac{A_{83}^{-1}A_{34}^{-1}}{A_{33}} & - & - & - & - \end{pmatrix}.
\end{aligned} \tag{A6}$$

Thus

$$\sigma_L^{outT} = \begin{pmatrix} 1 & 0 & -\frac{A_{31}^{-1}}{A_{33}} & 0 & 0 & 0 & 0 & 0 \\ 0 & 1 & -\frac{A_{32}^{-1}}{A_{33}} & 0 & 0 & 0 & 0 & 0 \\ 0 & 0 & \frac{1}{A_{33}} & 0 & 0 & 0 & 0 & 0 \\ 0 & 0 & -\frac{A_{34}^{-1}}{A_{33}} & 1 & 0 & 0 & 0 & 0 \\ 0 & 0 & -\frac{A_{35}^{-1}}{A_{33}} & 0 & 1 & 0 & 0 & 0 \\ 0 & 0 & -\frac{A_{36}^{-1}}{A_{33}} & 0 & 0 & 1 & 0 & 0 \\ 0 & 0 & -\frac{A_{37}^{-1}}{A_{33}} & 0 & 0 & 0 & 1 & 0 \\ 0 & 0 & -\frac{A_{38}^{-1}}{A_{33}} & 0 & 0 & 0 & 0 & 1 \end{pmatrix} \Rightarrow \sigma_L^{outT^{-1}} = \begin{pmatrix} 1 & 0 & A_{31}^{-1} & 0 & 0 & 0 & 0 & 0 \\ 0 & 1 & A_{32}^{-1} & 0 & 0 & 0 & 0 & 0 \\ 1 & 0 & A_{33} & 0 & 0 & 0 & 0 & 0 \\ 0 & 0 & A_{34}^{-1} & 1 & 0 & 0 & 0 & 0 \\ 0 & 0 & A_{35}^{-1} & 0 & 1 & 0 & 0 & 0 \\ 0 & 0 & A_{36}^{-1} & 0 & 0 & 1 & 0 & 0 \\ 0 & 0 & A_{37}^{-1} & 0 & 0 & 0 & 1 & 0 \\ 0 & 0 & A_{38}^{-1} & 0 & 0 & 0 & 0 & 1 \end{pmatrix} \tag{A7}$$

and

$$\sigma_L^{inT} = \begin{pmatrix} A_{11} - \frac{A_{13}A_{31}}{A_{33}} & A_{12} - \frac{A_{13}A_{32}}{A_{33}} & 0 & A_{14} - \frac{A_{13}A_{34}}{A_{33}} & - & - & - & - \\ A_{21} - \frac{A_{23}A_{31}}{A_{33}} & A_{22} - \frac{A_{23}A_{32}}{A_{33}} & 0 & A_{24} - \frac{A_{23}A_{34}}{A_{33}} & - & - & - & - \\ \frac{A_{13}}{A_{33}} & \frac{A_{23}}{A_{33}} & 1 & \frac{A_{43}}{A_{33}} & \frac{A_{53}}{A_{33}} & \frac{A_{63}}{A_{33}} & \frac{A_{73}}{A_{33}} & \frac{A_{83}}{A_{33}} \\ A_{41} - \frac{A_{43}A_{31}}{A_{33}} & A_{42} - \frac{A_{43}A_{32}}{A_{33}} & 0 & A_{44} - \frac{A_{43}A_{34}}{A_{33}} & - & - & - & - \\ \vdots & \vdots & \vdots & \vdots & \vdots & \vdots & \vdots & \vdots \\ A_{81} - \frac{A_{83}A_{31}}{A_{33}} & A_{82} - \frac{A_{83}A_{32}}{A_{33}} & 0 & A_{84} - \frac{A_{83}A_{34}}{A_{33}} & - & - & - & - \end{pmatrix}. \tag{A8}$$

Finally, by (37), we obtain the scattering matrix when there are 8 oscillatory mode-solutions on either side of the interface,

$$S_{8 \times 8} = \begin{pmatrix} A_{11} - \frac{A_{13}A_{31}}{A_{33}} & A_{21} - \frac{A_{23}A_{31}}{A_{33}} & -\frac{A_{31}}{A_{33}} & A_{41} - \frac{A_{43}A_{31}}{A_{33}} & - & - & - & - \\ A_{12} - \frac{A_{13}A_{32}}{A_{33}} & A_{22} - \frac{A_{23}A_{32}}{A_{33}} & -\frac{A_{32}}{A_{33}} & A_{42} - \frac{A_{43}A_{32}}{A_{33}} & - & - & - & - \\ \frac{A_{13}}{A_{33}} & \frac{A_{23}}{A_{33}} & \frac{1}{A_{33}} & \frac{A_{43}}{A_{33}} & - & - & - & - \\ A_{14} - \frac{A_{13}A_{34}}{A_{33}} & A_{24} - \frac{A_{23}A_{34}}{A_{33}} & -\frac{A_{34}}{A_{33}} & A_{44} - \frac{A_{43}A_{34}}{A_{33}} & - & - & - & - \\ \vdots & \vdots & \vdots & \vdots & \vdots & \vdots & \vdots & \vdots \\ A_{18} - \frac{A_{13}A_{38}}{A_{33}} & A_{28} - \frac{A_{23}A_{38}}{A_{33}} & -\frac{A_{38}}{A_{33}} & A_{48} - \frac{A_{43}A_{38}}{A_{33}} & - & - & - & - \end{pmatrix} \quad (\text{A9})$$

In (A9), we have completed the derivation of the S matrix for mode configuration 3, the frequency interval over which there are 8 oscillatory solutions to the field equations on either side of the interface, in terms of the amplitudes of the LMs on either side of the interface. This derivation followed from the matching conditions for the fields and their first spatial derivative at the interface and results in a straightforward expression that can easily be implemented — in Mathematica for the sake of the present paper.

### Appendix B: $\delta$ -function and frequency intervals in the moving- and laboratory-frame

In this appendix, we detail the treatment of the  $\delta$ -function used derivation of the photon-number Pearson

correlation coefficient in the moving- and laboratory-frame in section III B. We begin with the equations for the moving-frame covariance (45) and variance (46) — in which  $\delta_\epsilon(\omega'_1, \omega'_1) = \delta_\epsilon(0)$  — with

$$\delta_\epsilon(\omega') = \frac{1}{\epsilon}, |\omega'| \leq \frac{\epsilon}{2} \vee 0 \text{ otherwise} \quad (\text{B1})$$

such that  $\delta_\epsilon(0) = \frac{1}{\delta\omega'}$ . From Eq.(50), we see that

$$d\omega' = \gamma \left| 1 - \frac{u}{v_g(\omega)} \right| d\omega, \quad (\text{B2})$$

wherefrom  $\delta\omega' = \gamma \left| 1 - \frac{u}{v_g(\omega)} \right| \Delta\omega$ , which was used in calculating (53) and (54) from (45) and (46), respectively, yielding (55).